Fig. 3. Proposed model of regulation of blood flow in physiologicallystimulated human brain

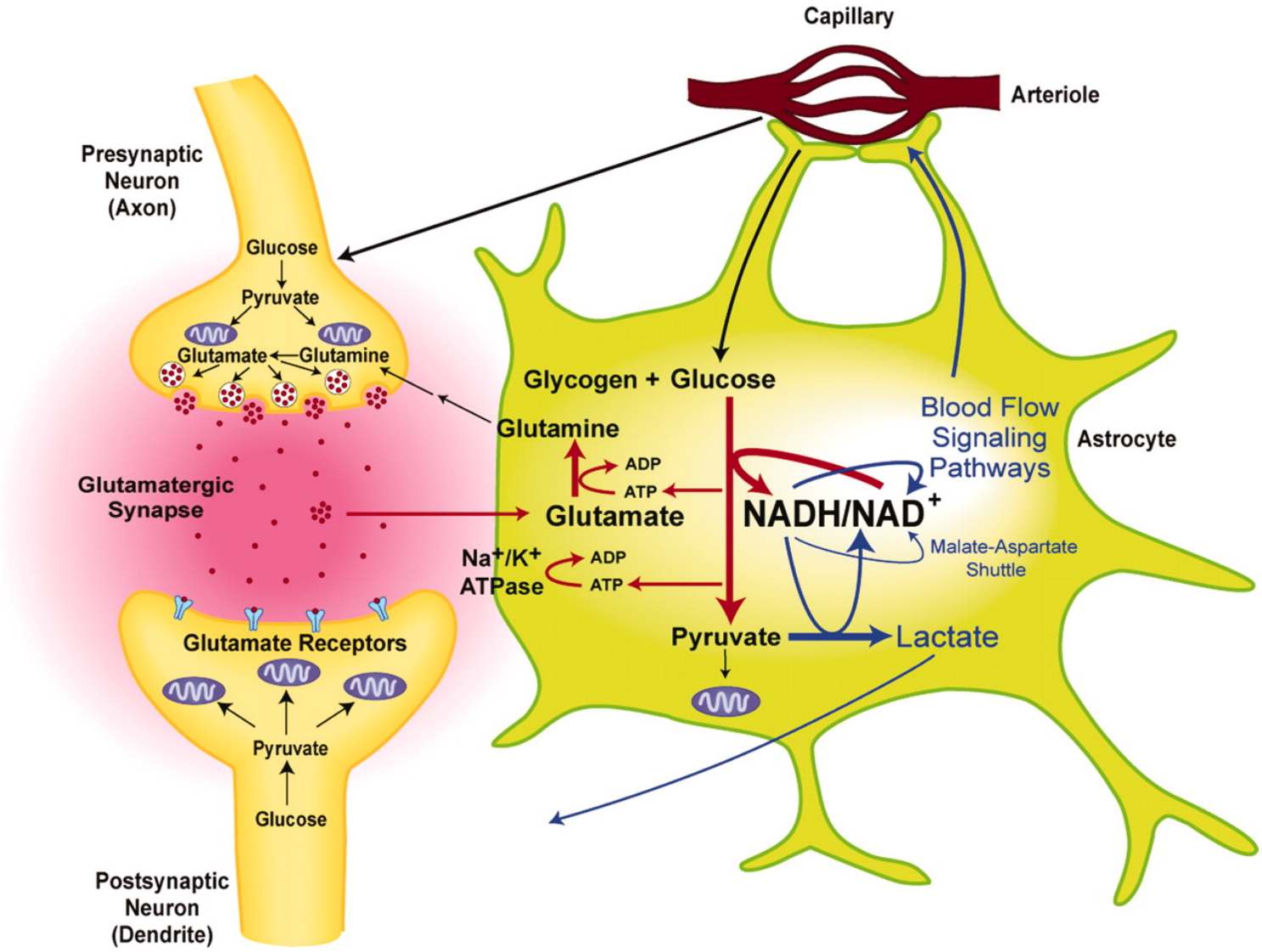

Vlassenko, Andrei G. et al. (2006) Proc. Natl. Acad. Sci. USA 103, 1964-1969

Rôle des Astrocytes dans le couplage neurométabolique

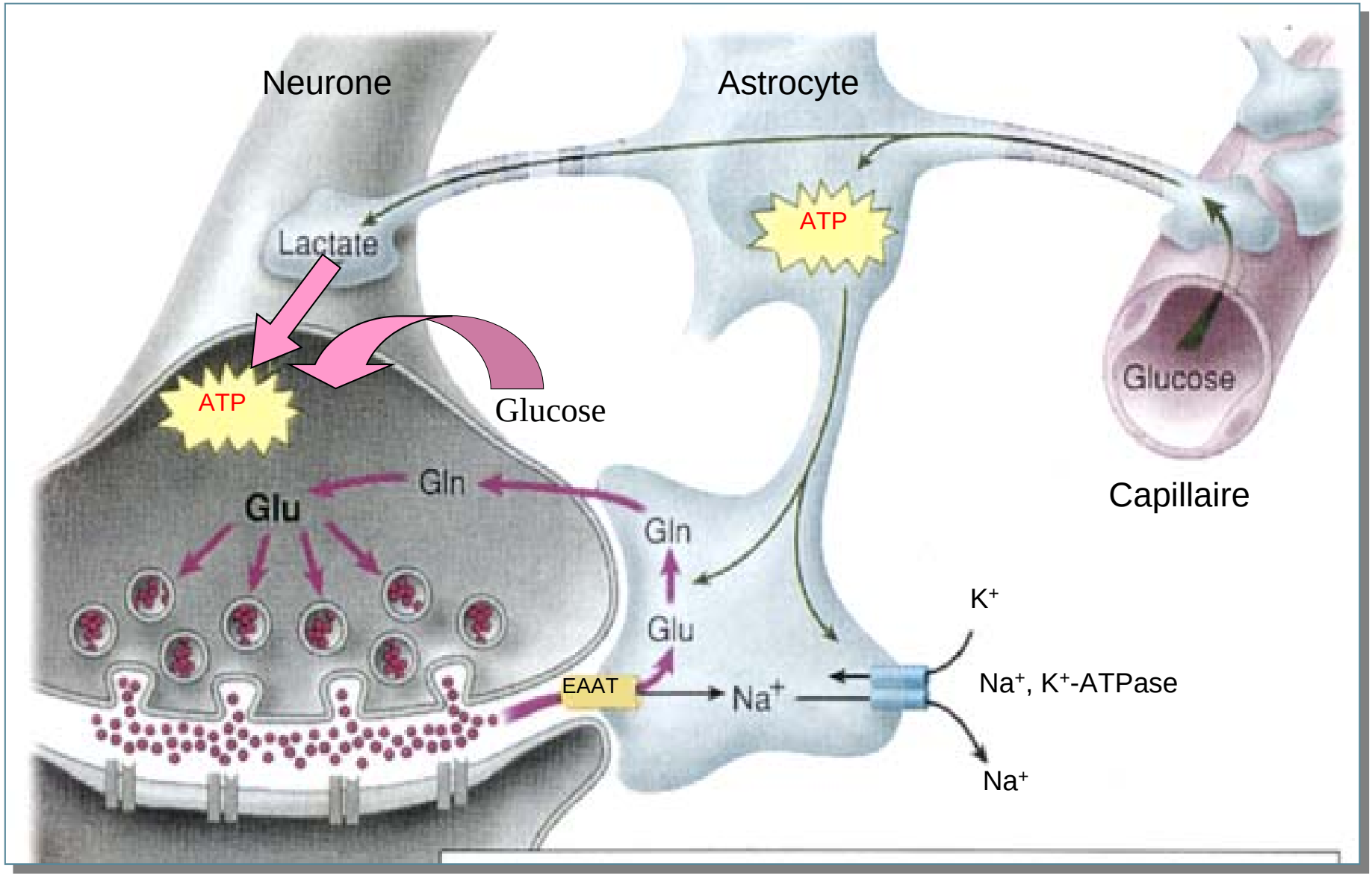

Neuroscience 141 (2006) 157–165

GLUCOSE AND LACTATE ARE EQUALLY EFFECTIVE IN ENERGIZING ACTIVITY-DEPENDENT SYNAPTIC VESICLE TURNOVER IN PURIFIED CORTICAL NEURONS

F. D. MORGENTHALER,[a1] R. KRAFTSIK,[b] S. CATSICAS,[c] P. J. MAGISTRETTI[a,e] AND J.-Y. CHATTON[a,b,d*]

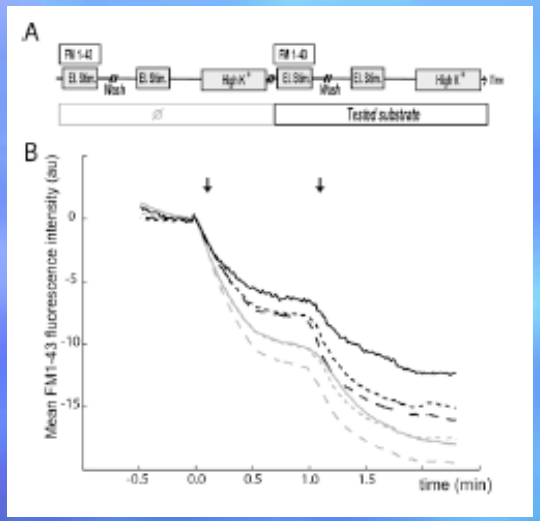

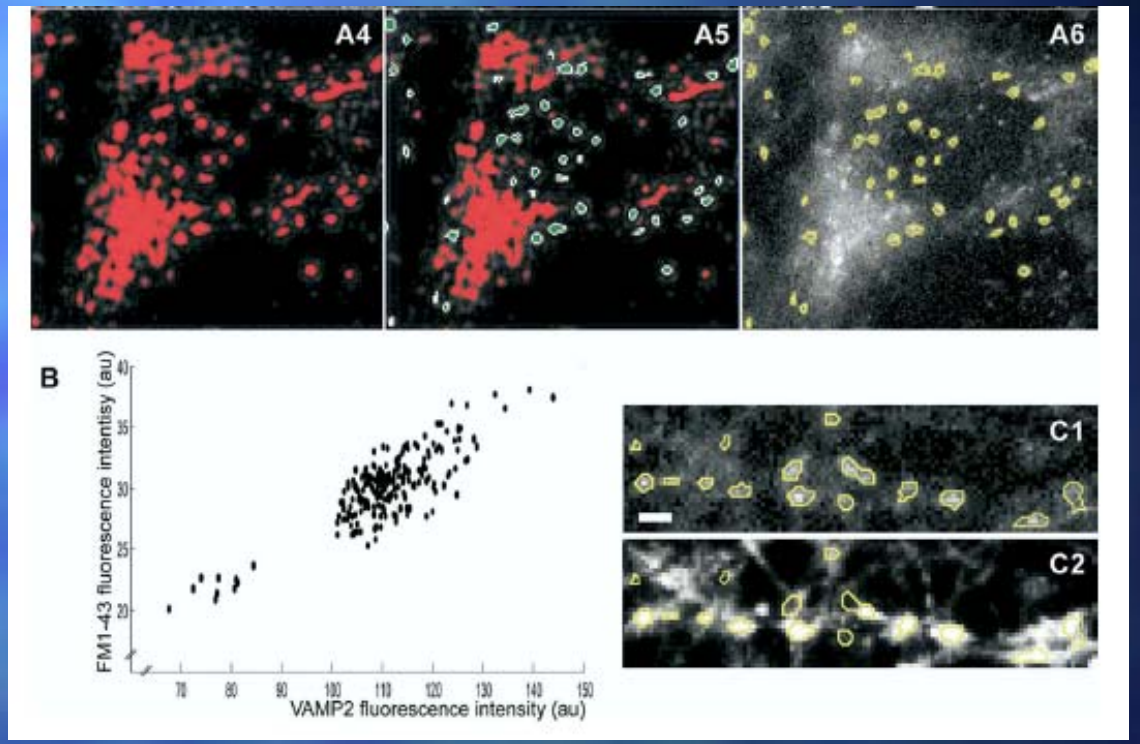

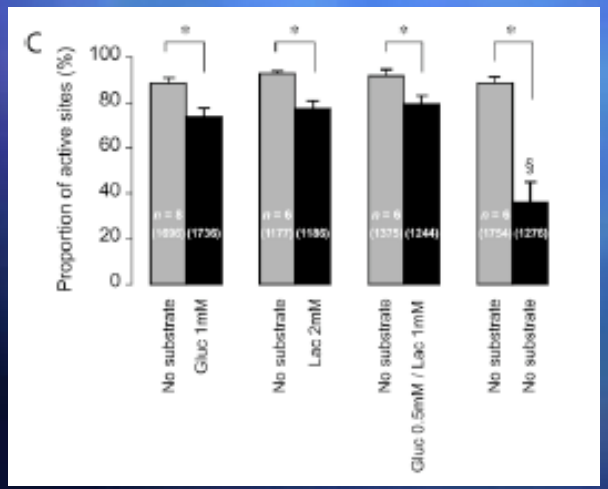

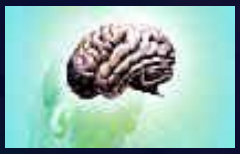

Neuron
Article

Glial Na_x Channels Control Lactate Signaling to Neurons for Brain [Na^+] Sensing

Hidetada Shimizu,[1,3,7] Eiji Watanabe,[2,3,7] Takeshi Y. Hiyama,[1,3,7] Ayano Nagakura,[1,3] Akihiro Fujikawa,[1] Haruo Okado,[4] Yuchio Yanagawa,[5] Kunihiko Obata,[6] and Masaharu Noda[1,3,*]

rons in the SFO. These results suggest that the information on a physiological increase of the Na level in body fluids sensed by Na_x in glial cells is transmitted to neurons by lactate as a mediator to regulate neural activities of the SFO.

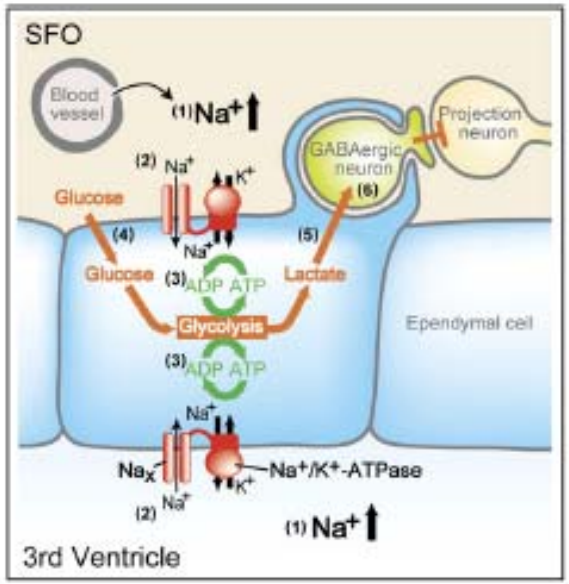

Figure 8. Schematic Overview of the Na-Level-Sensing Mechanism and Na-Dependent Regulation of Neurons in the SFO

Shimizu et al, Neuron 54, 59 - 72, 2007

4888 • The Journal of Neuroscience, May 7, 2008 • 28(19):4888–4896

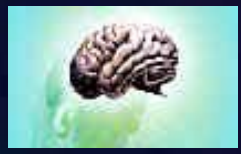

Cellular/Molecular

Inhibition of Monocarboxylate Transporter 2 in the Retrotrapezoid Nucleus in Rats: A Test of the Astrocyte–Neuron Lactate-Shuttle Hypothesis

Joseph S. Erlichman,[1] Amy Hewitt,[1] Tracey L. Damon,[1] Michael Hart,[1] Jennifer Kurascz,[1] Aihua Li,[2] and James C. Leiter[2]

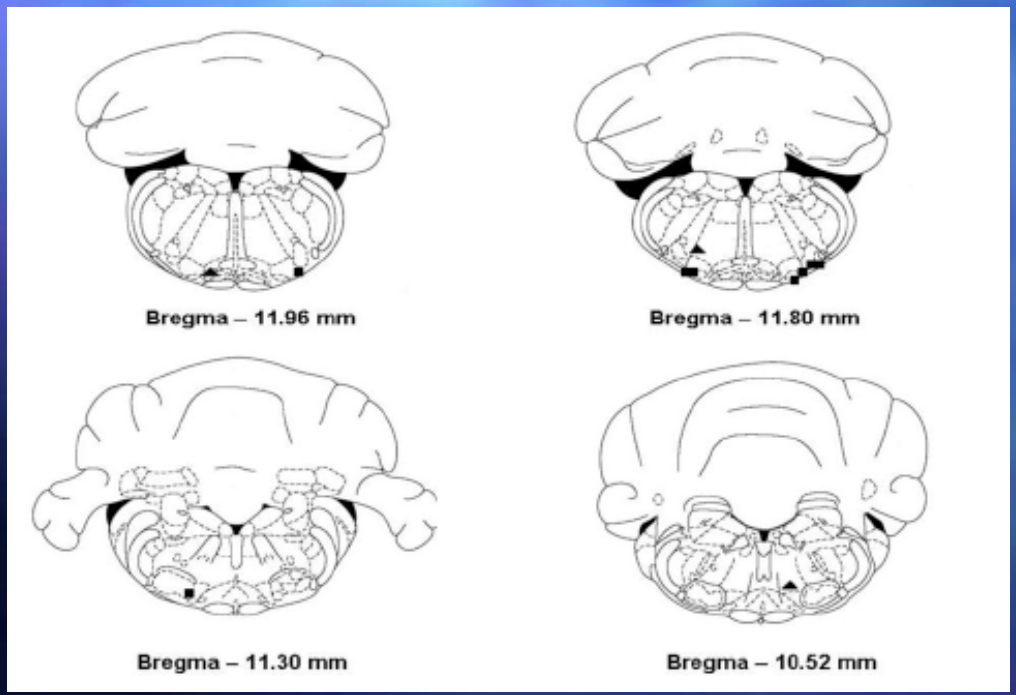

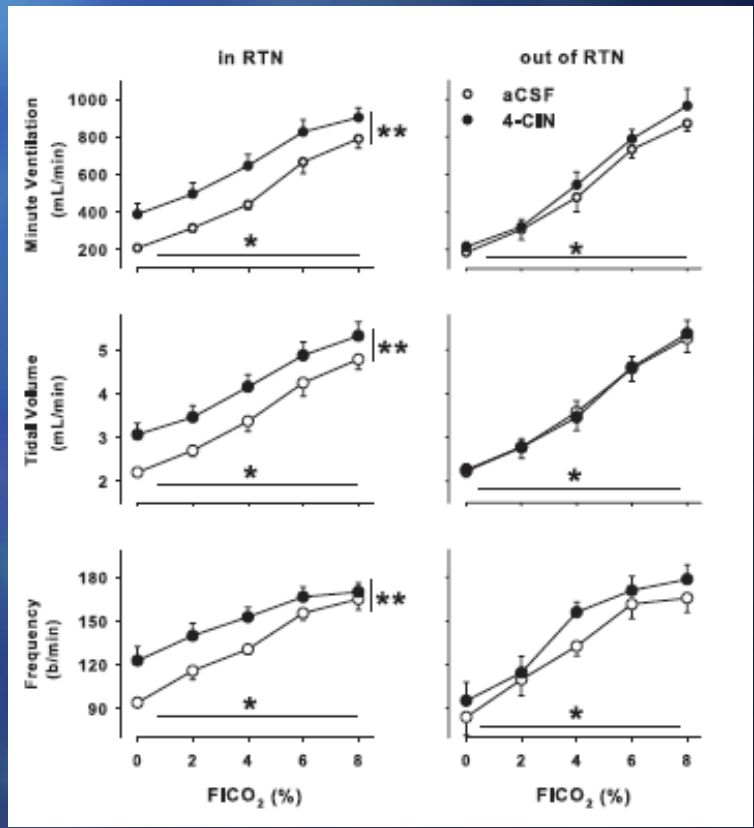

Rôle des astrocytes dans la production des signaux détectés par imagerie fonctionnelle

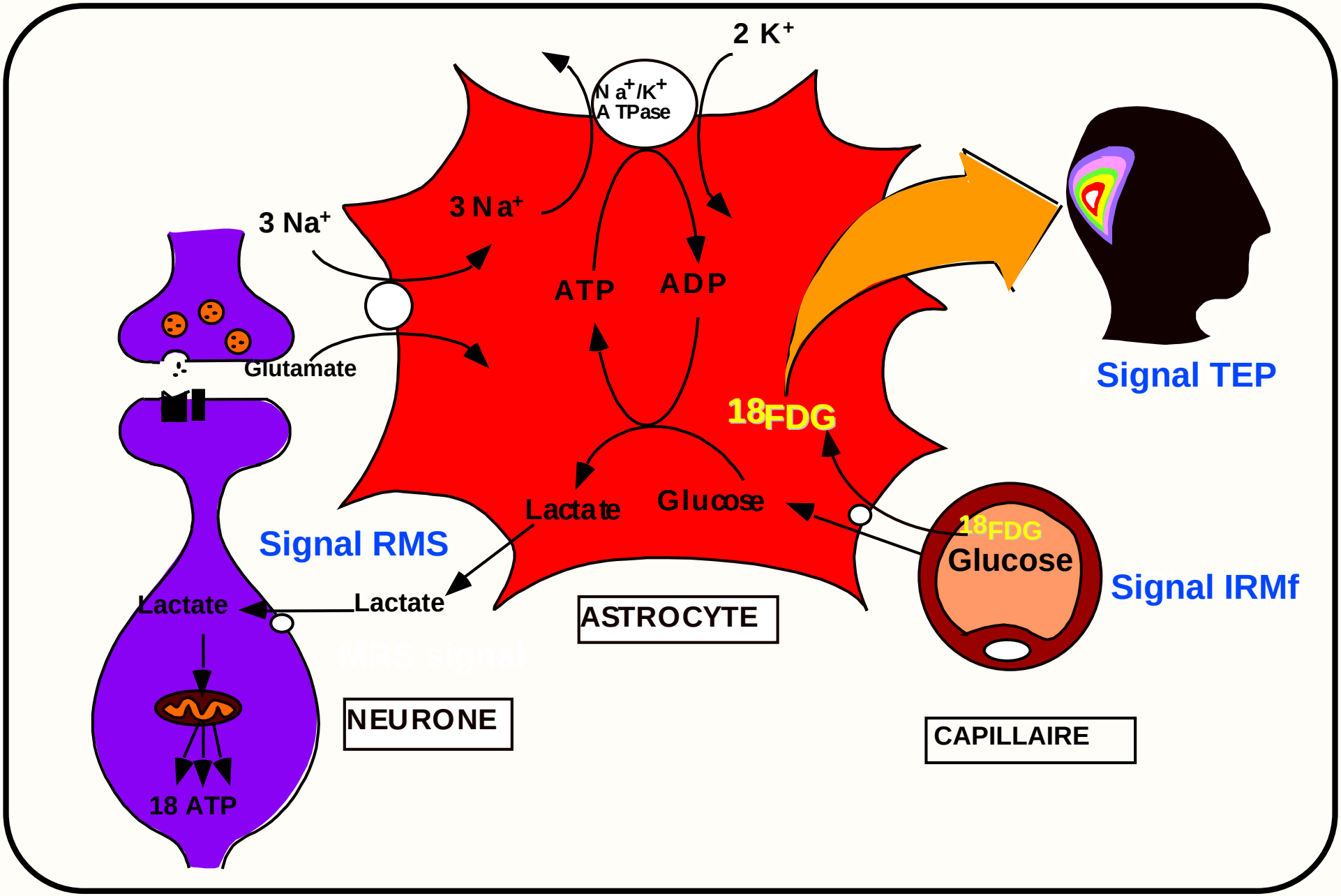

Longueur des axones :
neurones GABA : 1.5 Km
neuroneg glutamate : 40 Km

Neurones GABA :
Vm moins - , activables ++

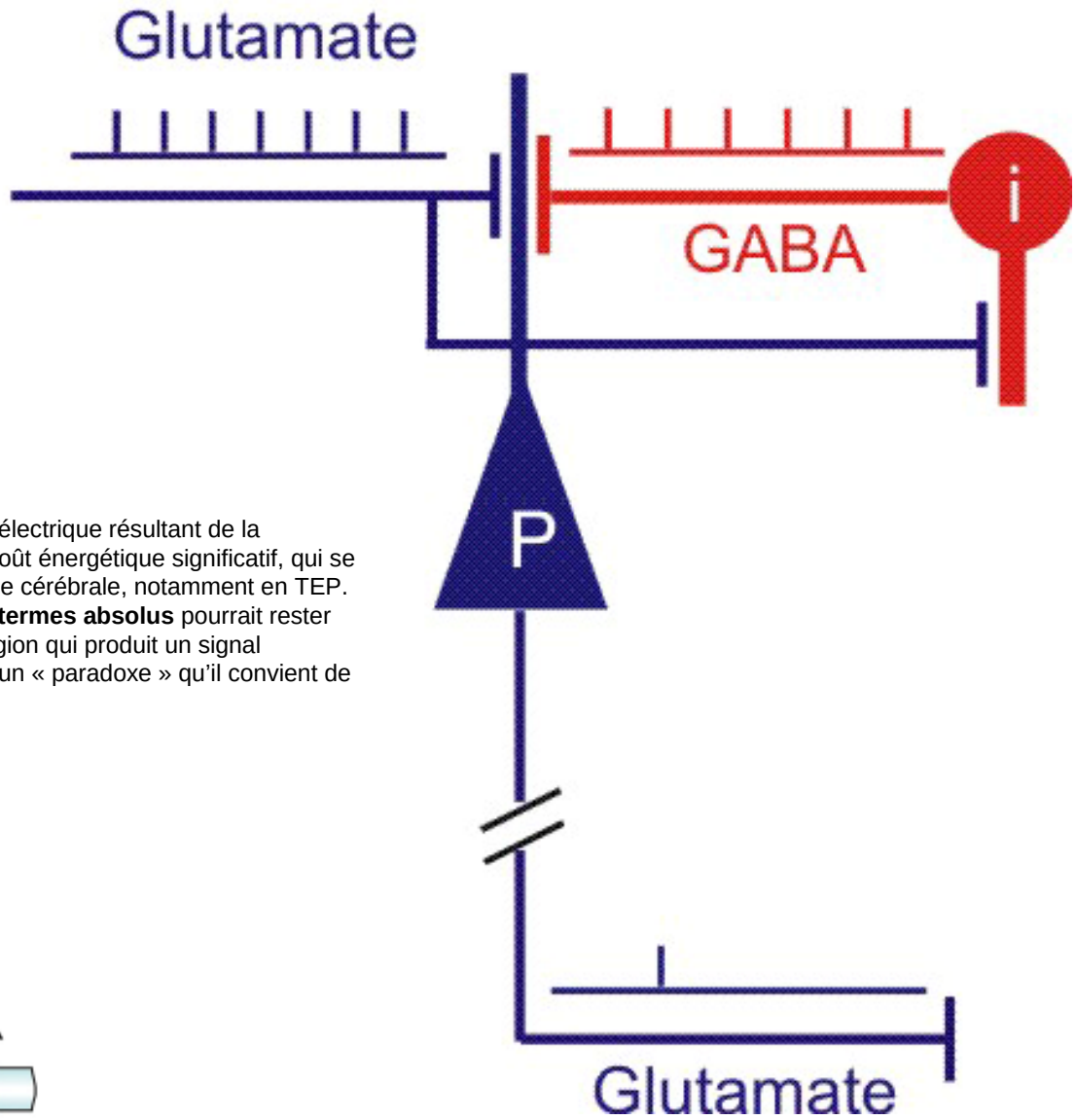

“Le point important est donc que même en l’absence d’activité électrique résultant de la convergence d’entrées excitatrices et inhibitrices, il y aura un coût énergétique significatif, qui se traduira par une image « d’activation » en imagerie fonctionnelle cérébrale, notamment en TEP. Voilà pourquoi la question du coût de l’inhibition considéré **en termes absolus** pourrait rester sans réponse et signifier que en imagerie fonctionnelle, une région qui produit un signal métabolique, pourrait en fait être inhibée et non activée ! Voilà un « paradoxe » qu’il convient de considérer.” PJM, LI CdF 14.02.08

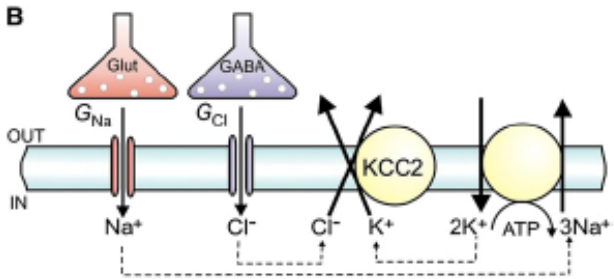

Buzsaki et al 2007

Vagues intercellulaires calciques, sodiques et métaboliques

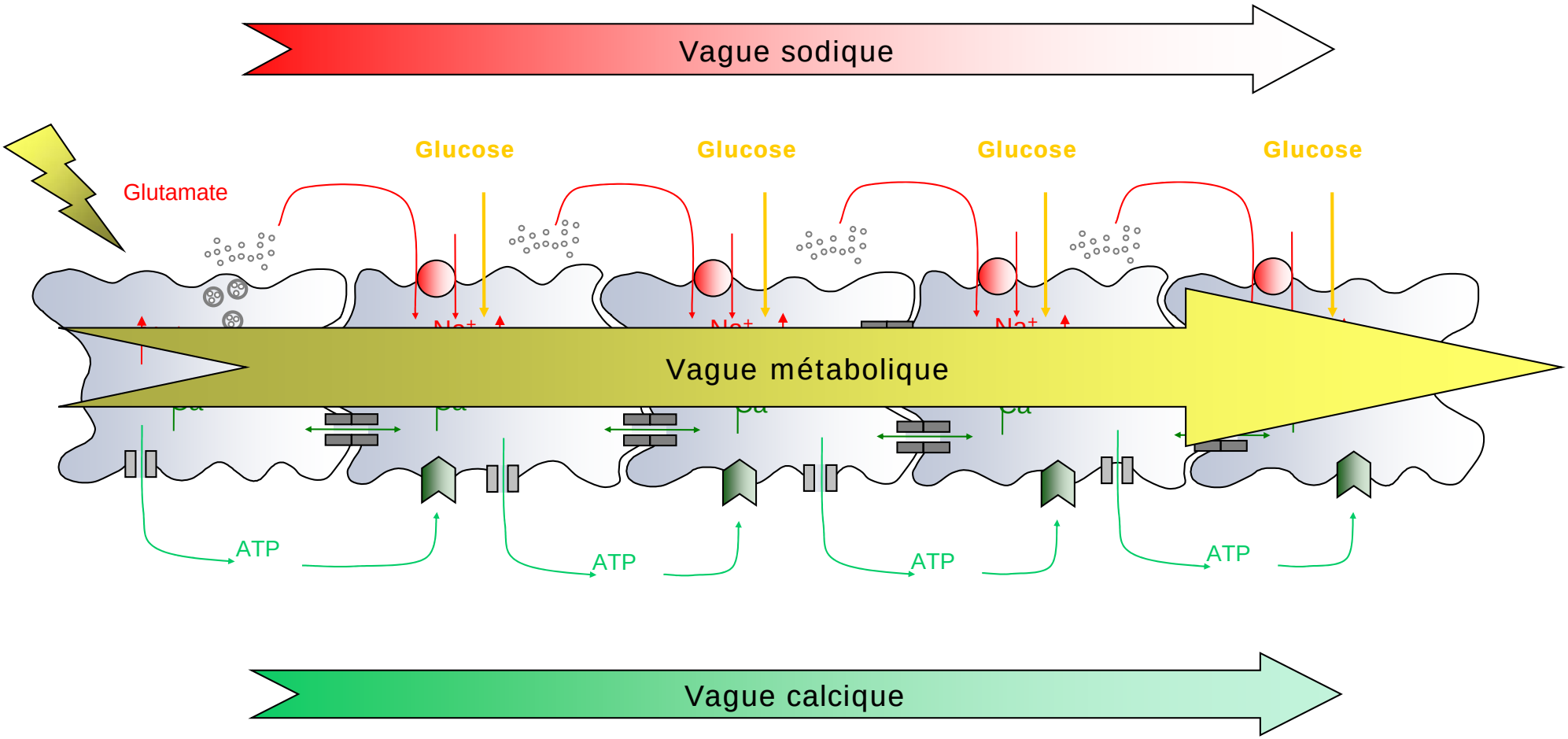

Mécanisme d’amplification du couplage neurométabolique

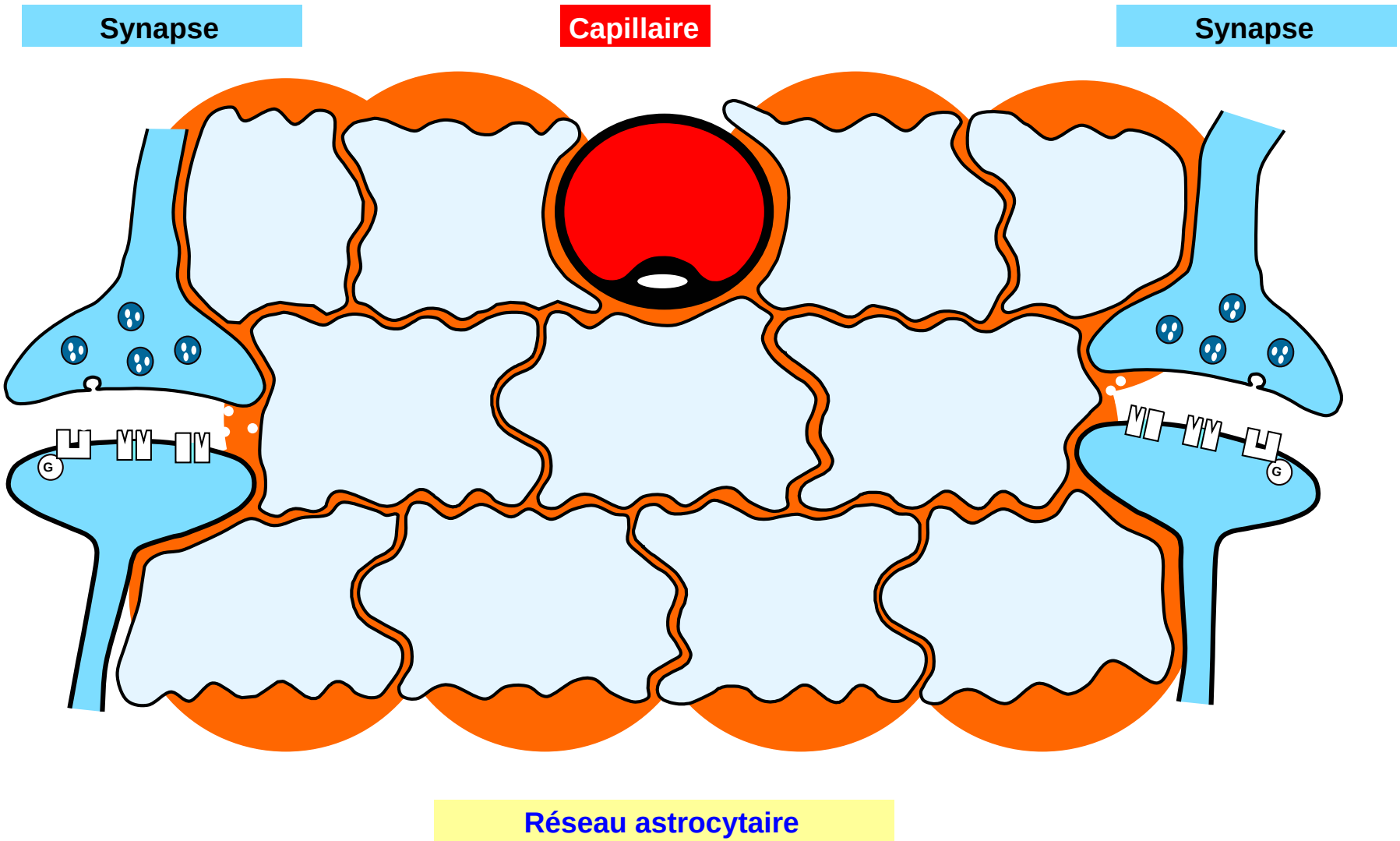

Rôle des astrocytes dans la production des signaux détectés par imagerie fonctionnelle

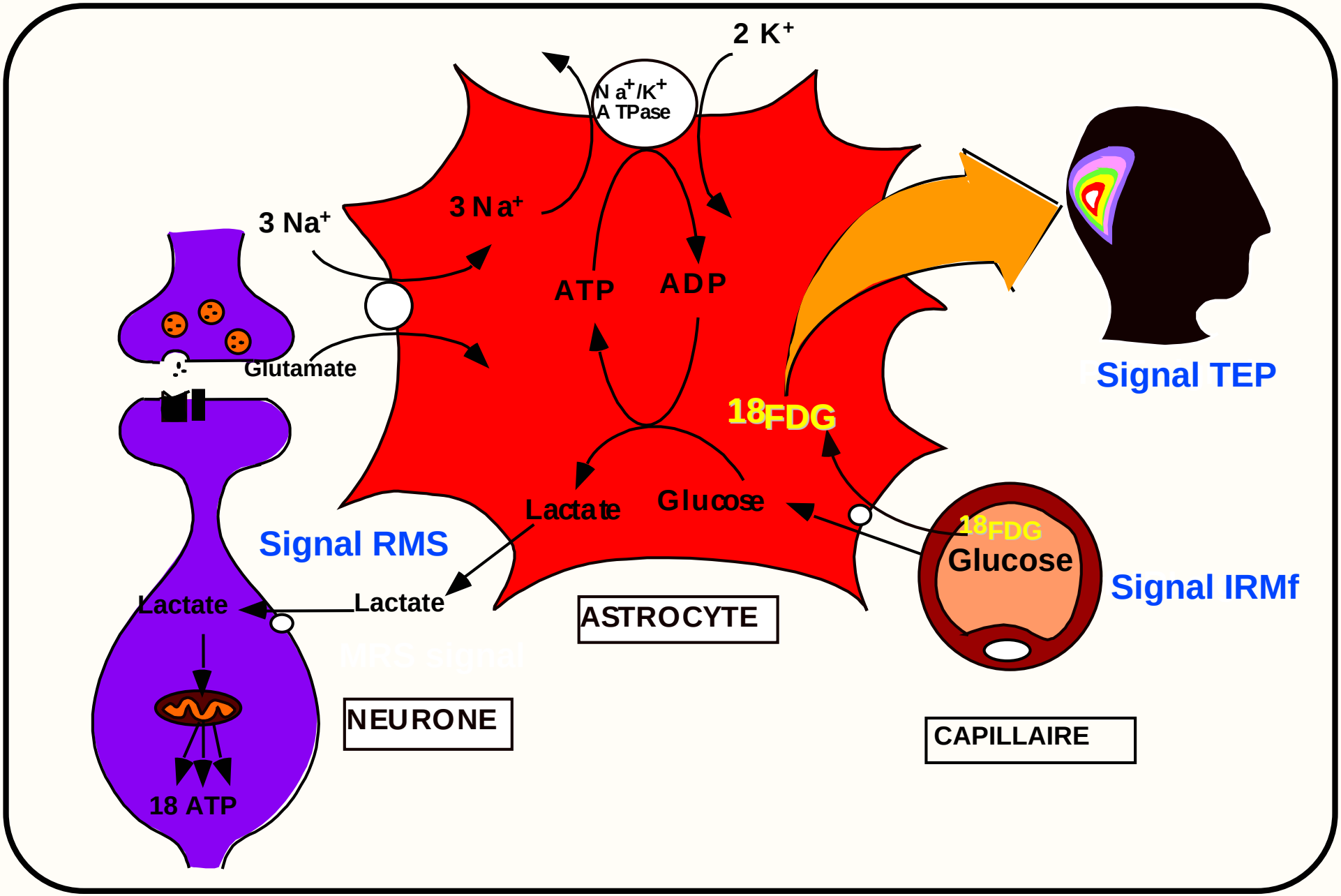

Réponses neurométaboliques et neurovasculaires durant l'activation

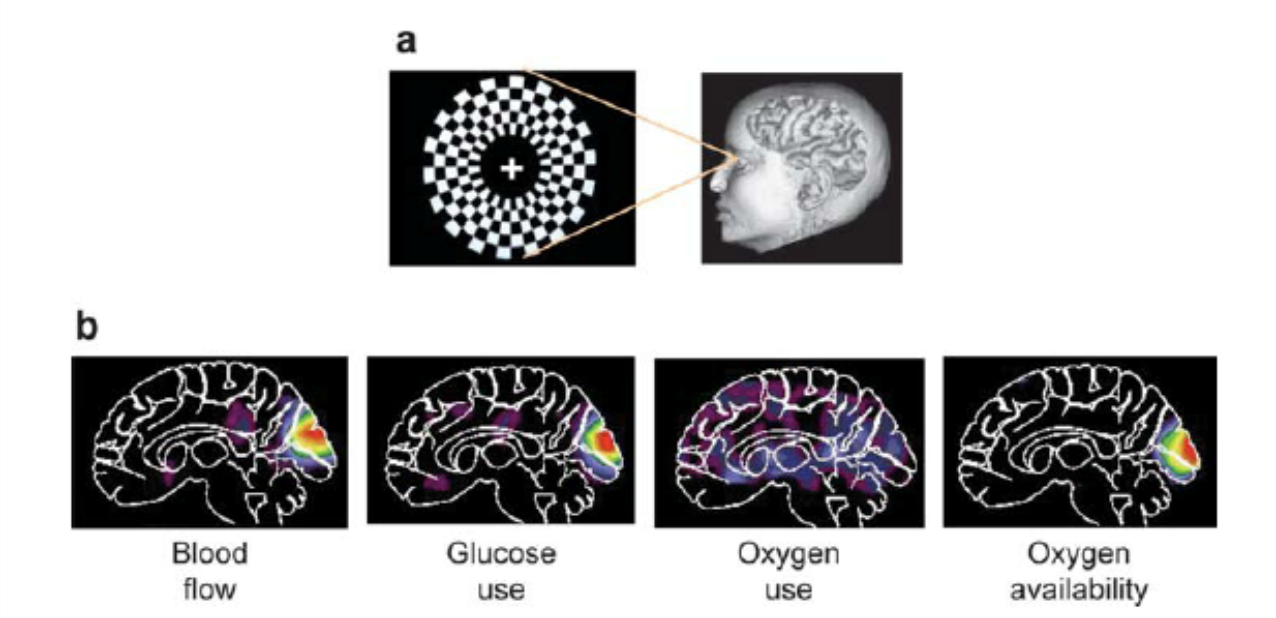

Raichle et Mintun, 2006

Débit sanguin, consommation d'oxygène et fraction d'extraction d'oxygène pendant une stimulation visuelle

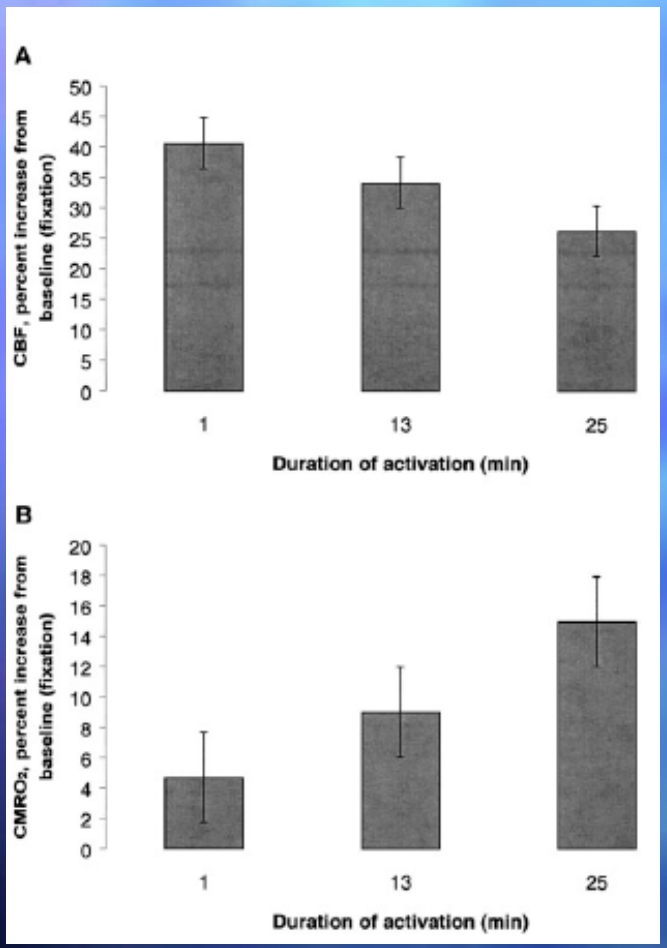

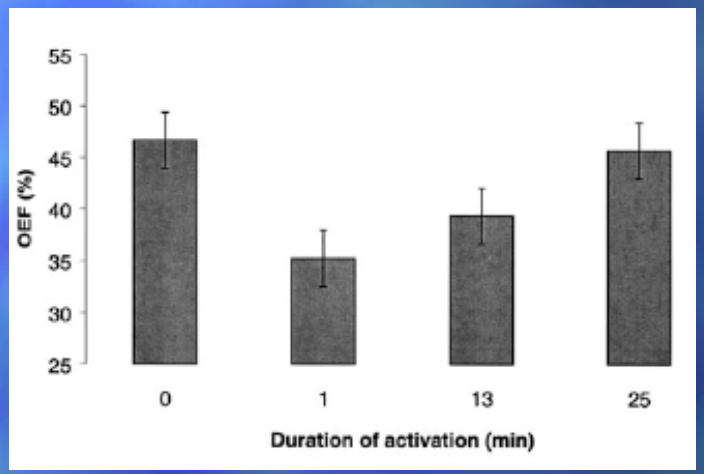

Mintun et al 2002

Analyse du signal BOLD : activations et déactivations

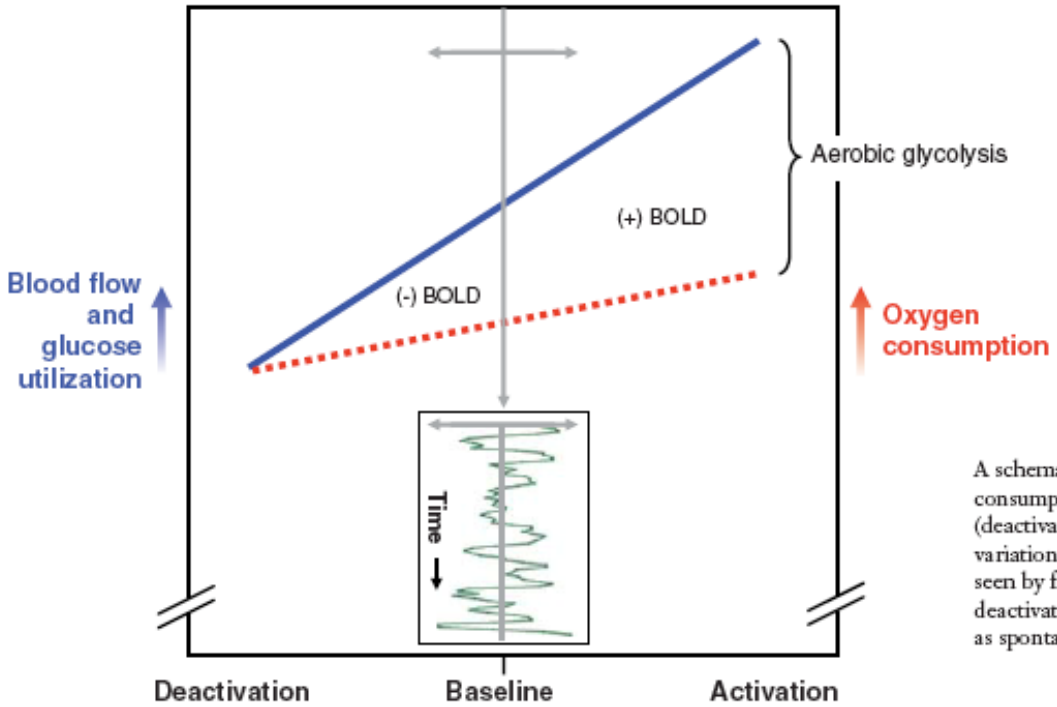

A schematic representation of the relationship of blood flow and glucose utilization (*blue*) to oxygen consumption (*red*) and cellular activity (*x-axis*) at baseline and during increases (activation) and decreases (deactivation) in neuronal activity. The presence of aerobic glycolysis causes activity-dependent variations in oxygen availability in the brain (see **Figure 1**) that are detectable by fMRI. Activations as seen by fMRI result from a disproportionate increase in blood flow and glucose utilization, whereas deactivations result from the opposite. At baseline, time-varying fluctuations in neuronal activity are seen as spontaneous fluctuations in the fMRI BOLD signal (*insert, green line*).

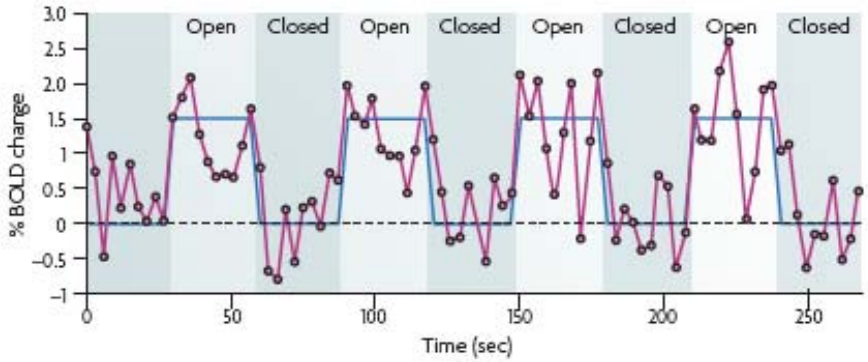

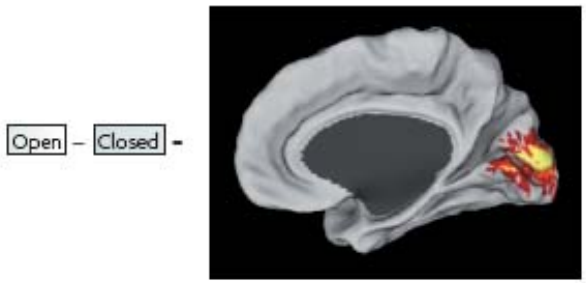

Raichle et Mintun 2007 **Fox et Raichle, 2007**

Le mode par défaut “default mode” de l’activité cérébrale

Aires principales :
- cortex préfrontal médian
- cingulaire postérieur
- pré-cunéus
- zones du cortex pariétal (latéral et médian)

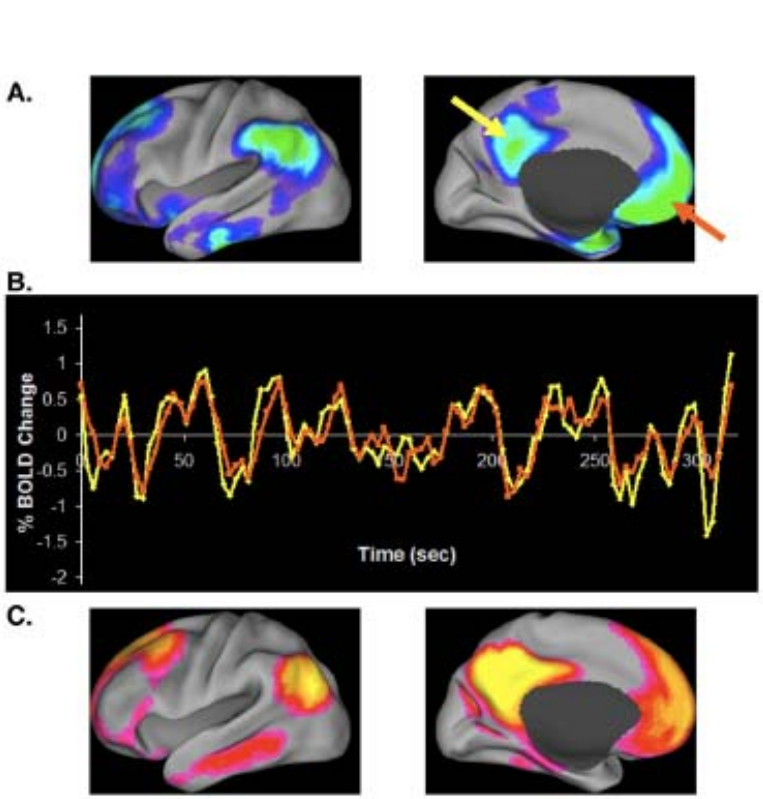

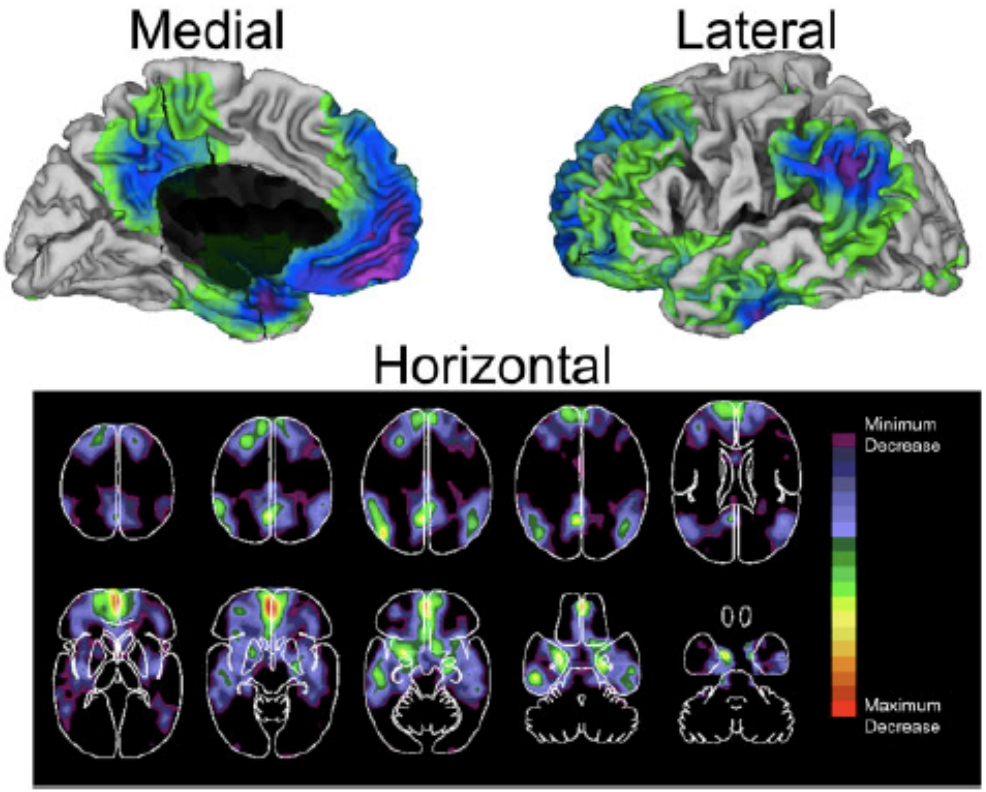

Raichle et Gusnard, 2005; Raichle et Snyder 2007

Fig. 1. Intrinsic correlations between a seed region in the PCC and all other voxels in the brain for a single subject during resting fixation

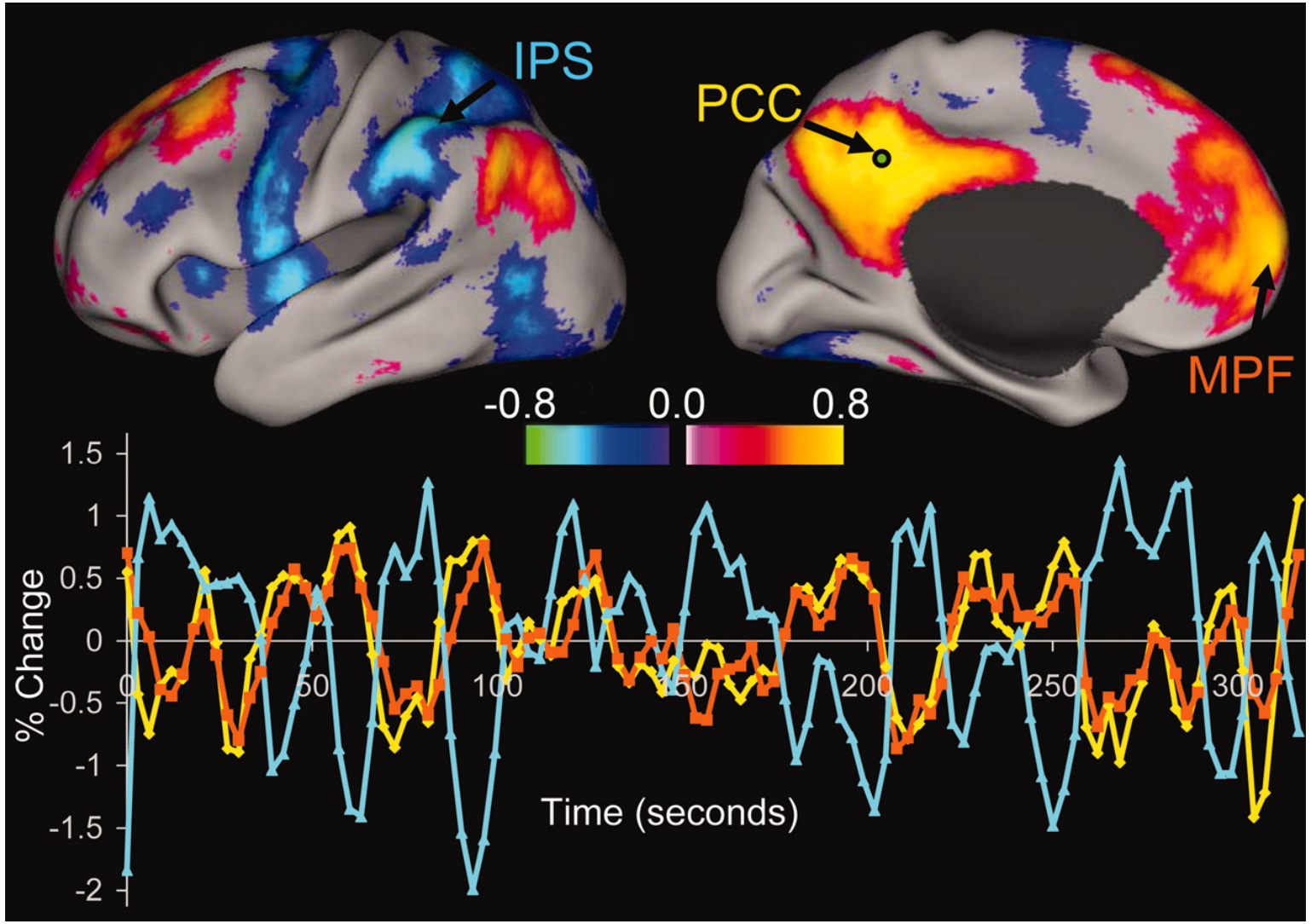

Fox, Michael D. et al. (2005) Proc. Natl. Acad. Sci. USA 102, 9673-9678

Fig. 1. Intrinsic correlations between a seed region in the PCC and all other voxels in the brain for a single subject during resting fixation. The spatial distribution of correlation coefficients shows both correlations (positive values) and anticorrelations (negative values), thresholded at $R = 0.3$. The time course for a single run is shown for the seed region (PCC, yellow), a region positively correlated with this seed region in the MPF (orange), and a region negatively correlated with the seed region in the IPS (blue).

Abbreviations: fMRI, functional MRI; BOLD, blood oxygen level-dependent; IPS, intraparietal sulcus; FEF, frontal eye field; MT+, middle temporal region; MPF, medial prefrontal cortex; PCC, posterior cingulate/precuneus; LP, lateral parietal cortex; SMA, supplementary motor area.

In recent years, the brain's "default network," a set of regions characterized by decreased neural activity during goal-oriented tasks, has generated a significant amount of interest, as well as controversy. Much of the discussion has focused on the relationship of these regions to a "default mode" of brain function. In early studies, investigators suggested that, the brain's default mode supports "self-referential" or "introspective" mental activity. Subsequently, regions of the default network have been more specifically related to the "internal narrative," the "autobiographical self," "stimulus independent thought," "mentalizing," and most recently "self-projection." However, the extant literature on the function of the default network is limited to adults, i.e., after the system has reached maturity. We hypothesized that further insight into the network's functioning could be achieved by characterizing its development. In the current study, we used resting-state functional connectivity MRI (rs-fcMRI) to characterize the development of the brain's default network. We found that the default regions are only sparsely functionally connected at early school age (7–9 years old); over development, these regions integrate into a cohesive, interconnected network.

Fair, Damien A. et al. (2008) Proc. Natl. Acad. Sci. USA 105, 4028-4032

Fig. 1. Voxelwise resting-state functional connectivity maps for a seed region (solid black circle) in mPFC (ventral: -3, 39, -2)

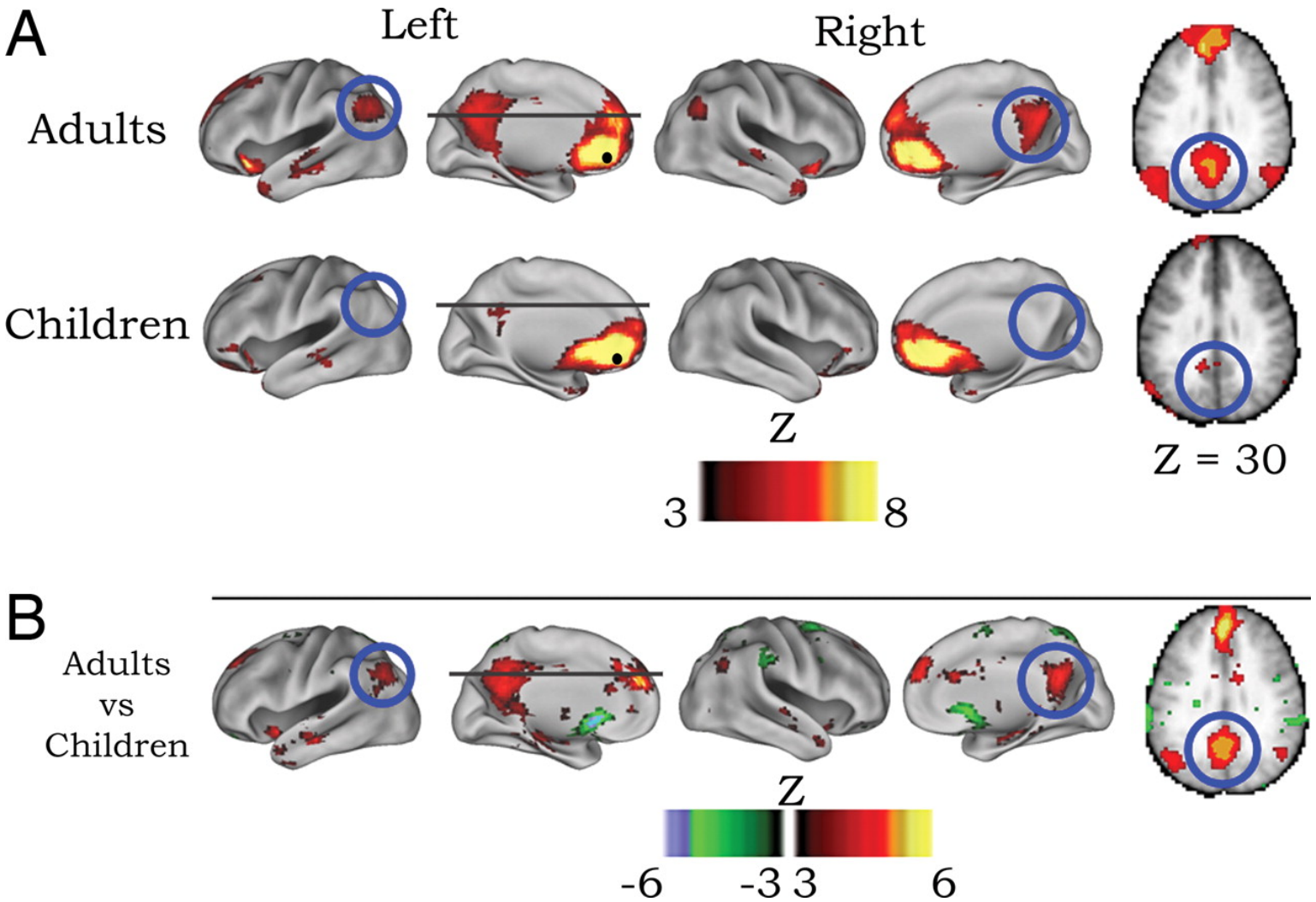

Fair, Damien A. et al. (2008) Proc. Natl. Acad. Sci. USA 105, 4028-4032

Fig. 3. Graph visualization of the correlation matrices shown in Fig

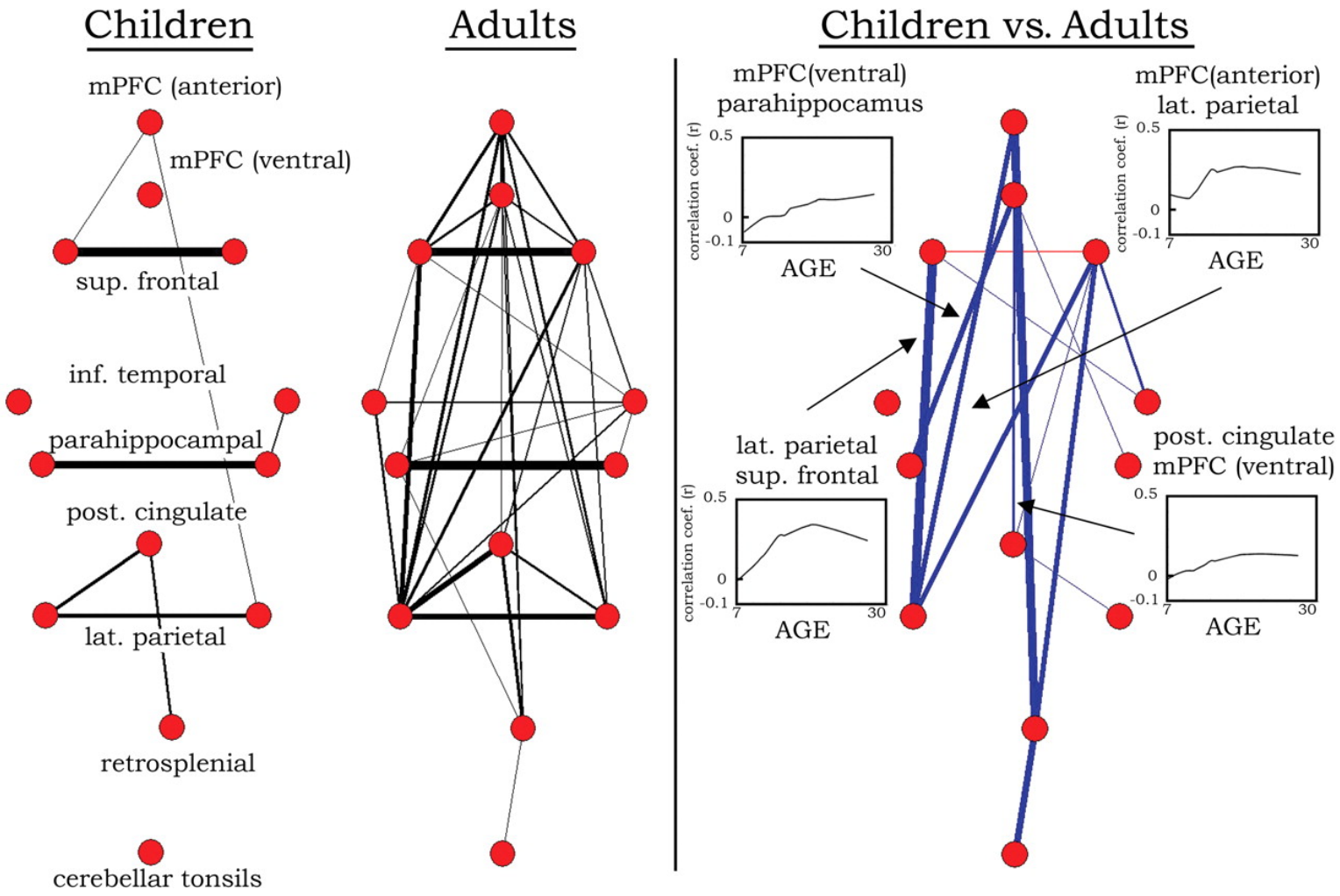

Fair, Damien A. et al. (2008) Proc. Natl. Acad. Sci. USA 105, 4028-4032

Young adults typically deactivate specific brain regions during active task performance. Deactivated regions overlap with those that show reduced resting metabolic activity in aging and dementia, raising the possibility of a relation. Here, the magnitude and dynamic temporal properties of these typically deactivated regions were explored in aging by using functional MRI in 82 participants. Young adults ($n = 32$), older adults without dementia ($n = 27$), and older adults with early-stage dementia of the Alzheimer type (DAT) ($n = 23$) were imaged while alternating between blocks of an active semantic classification task and a passive fixation baseline. Deactivation in lateral parietal regions was equivalent across groups; in medial frontal regions, it was reduced by aging but was not reduced further by DAT. Of greatest interest, a medial parietal/posterior cingulate region showed differences between young adults and older adults without dementia and an even more marked difference with DAT. The temporal profile of the medial parietal/posterior cingulate response suggested that it was initially activated by all three groups, but the response in young adults quickly reversed sign, whereas DAT individuals maintained activation throughout the task block. Exploratory whole-brain analyses confirmed the importance of medial parietal/posterior cingulate cortex differences in aging and DAT. These results introduce important opportunities to explore the functional properties of regions showing deactivations, how their dynamic functional properties relate to their baseline metabolic rates, and how they change with age and dementia.

Lustig, Cindy et al. (2003) Proc. Natl. Acad. Sci. USA 100, 14504-14509

Fig. 1. Regional analyses showing effects of age and dementia

Cortex frontal gauche

Cortex pariétal latéral droit

Cortex frontal médian

Cortex cingulaire postérieur
Cortex pariétal médian

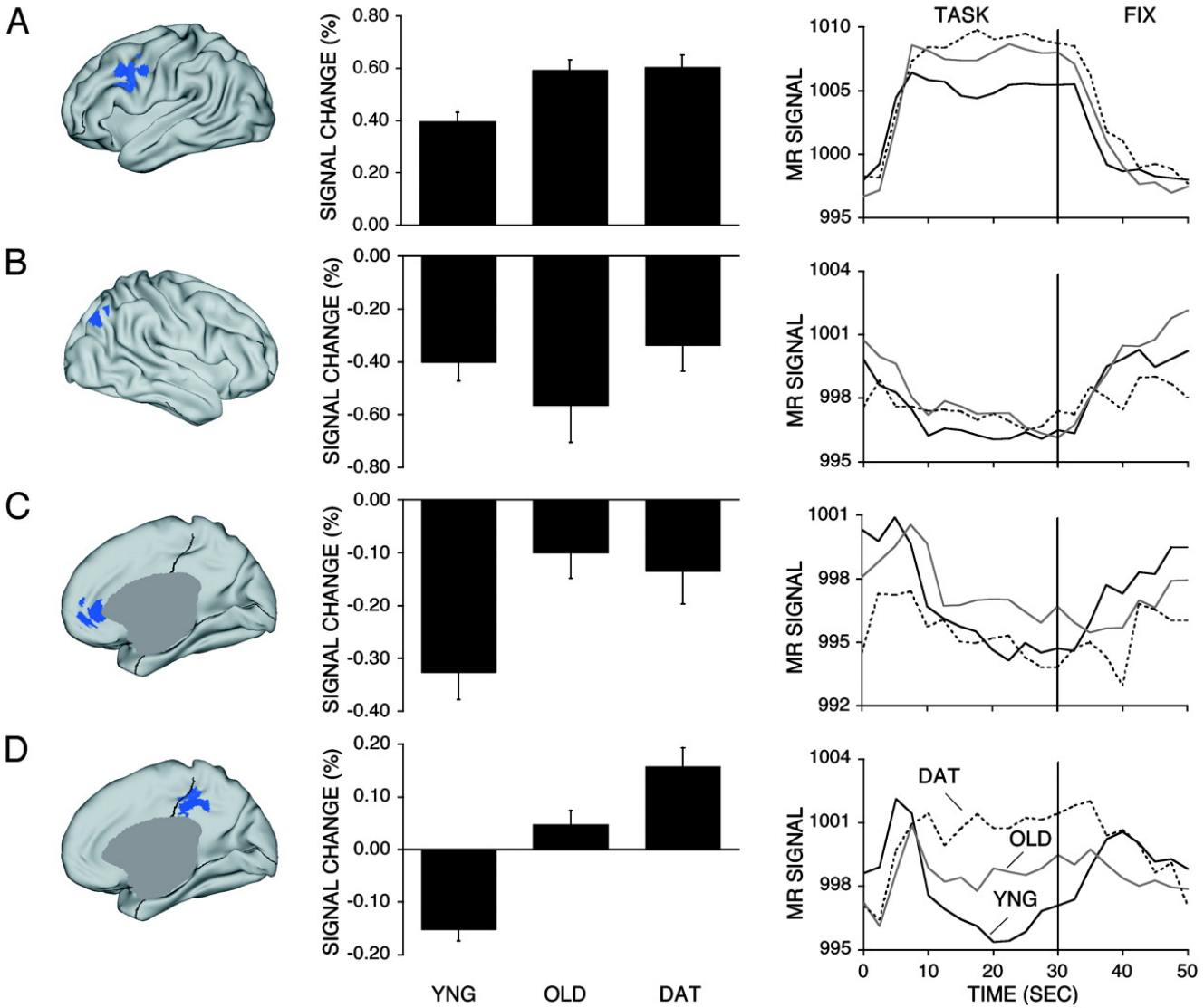

Lustig, Cindy et al. (2003) Proc. Natl. Acad. Sci. USA 100, 14504-14509

Fig. 2. Statistical activation maps for young, old, and DAT groups

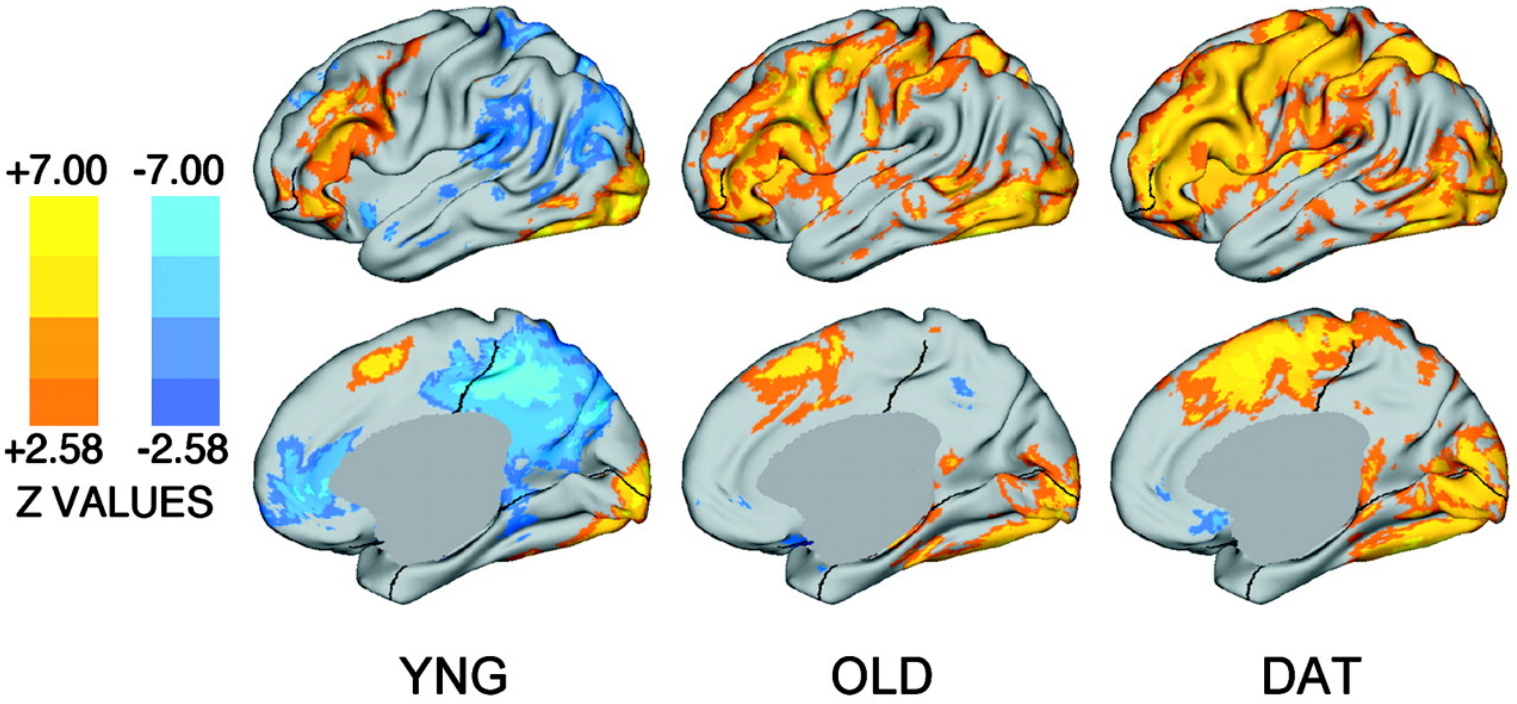

Lustig, Cindy et al. (2003) Proc. Natl. Acad. Sci. USA 100, 14504-14509

Rôle des astrocytes dans le couplage entre activité synaptique et métabolisme cérébral

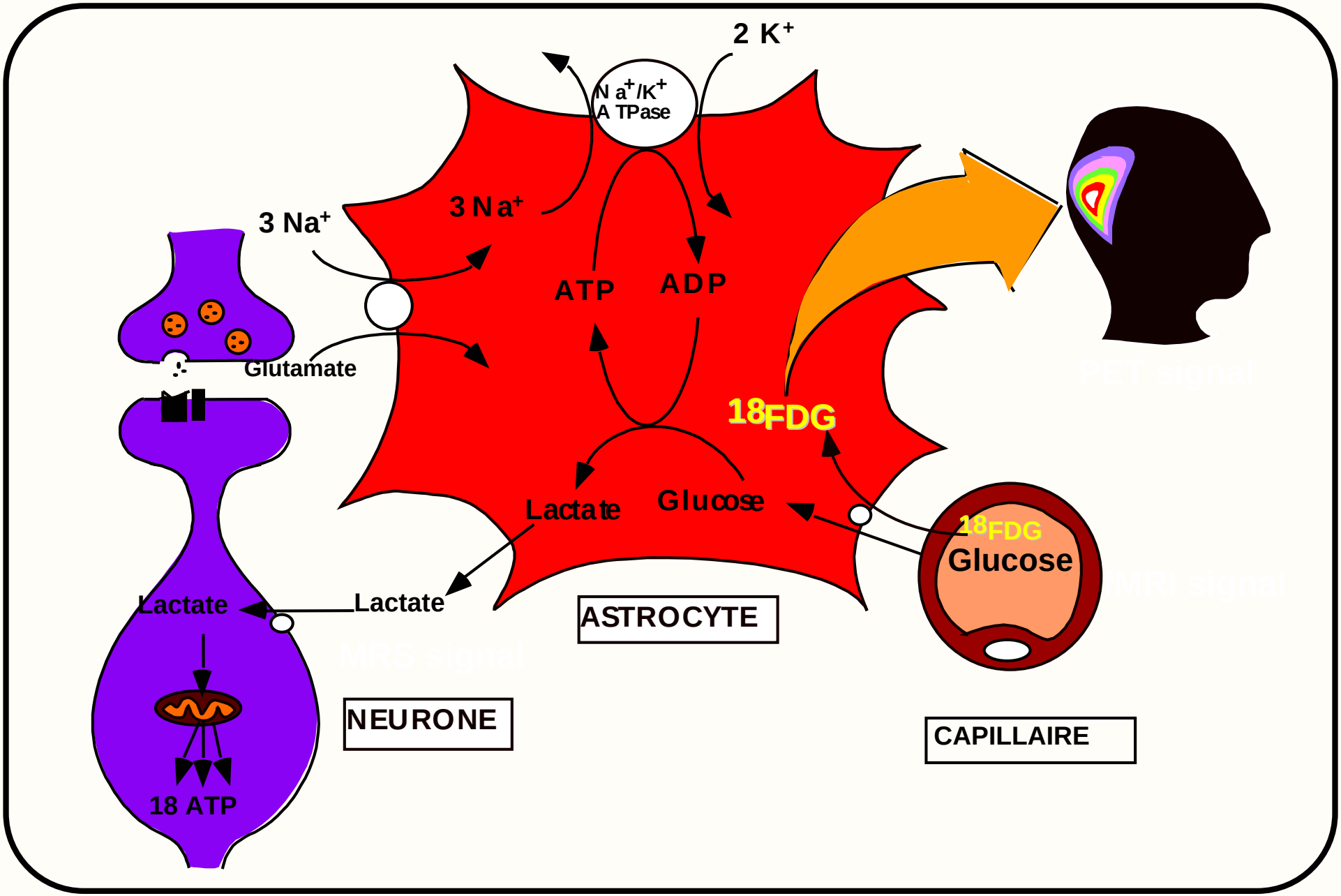

NORMAL BRAIN

ALZHEIMER'S BRAIN

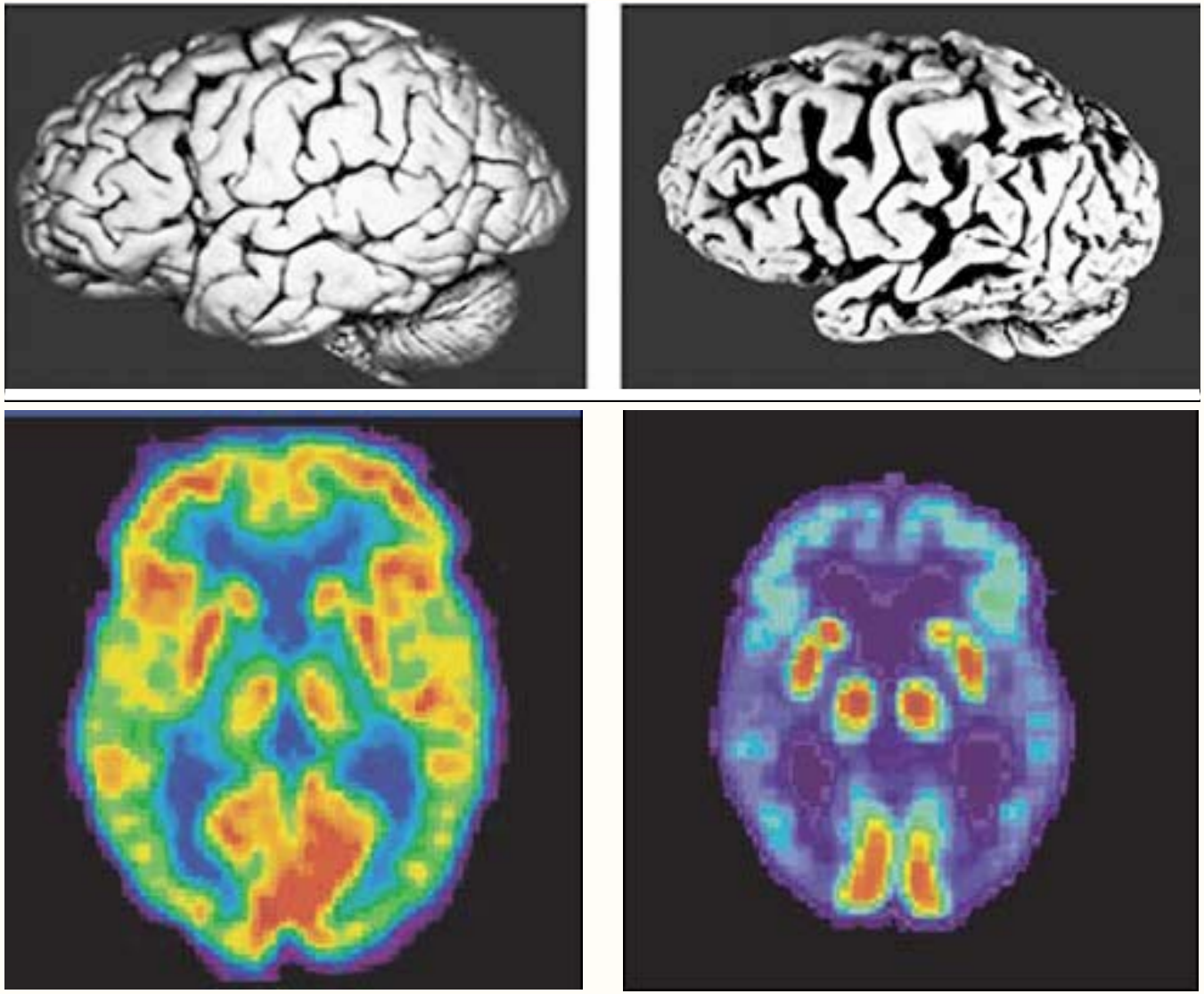

NORMAL BRAIN

ALZHEIMER'S BRAIN

PET scans (utilisation de glucose)

Mattson, Nature, 2004

PET scans (utilisation de glucose)

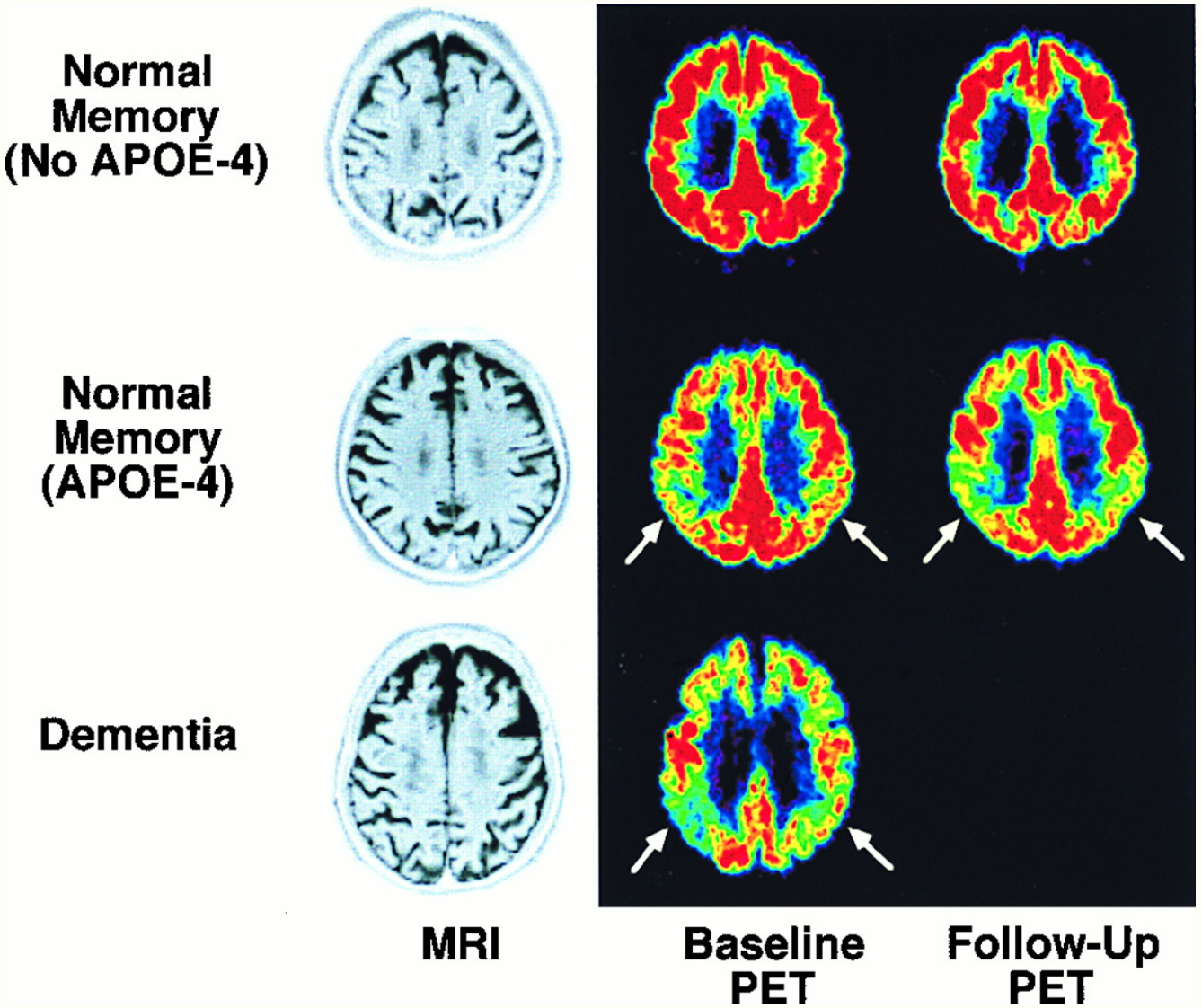

Small, Gary W. et al. (2000) Proc. Natl. Acad. Sci. USA 97, 6037-6042

Alzheimer's disease is associated with reduced expression of energy metabolism genes in posterior cingulate neurons

Winnie S. Liang*†, Eric M. Reiman*†‡§, Jon Valla†¶, Travis Dunckley*† Thomas G. Beach†‖, Andrew Grover†‖, Tracey L. Niedzielko†¶, Lonnie E. Schneider†¶, Diego Mastroeni†‖, Richard Caselli†**, Walter Kukull††, John C. Morris‡‡, Christine M. Hulette§§, Donald Schmechel§§, Joseph Rogers†‖, and Dietrich A. Stephan*†¶¶

PNAS | March 18, 2008 | vol. 105 | no. 11 | 4441–4446

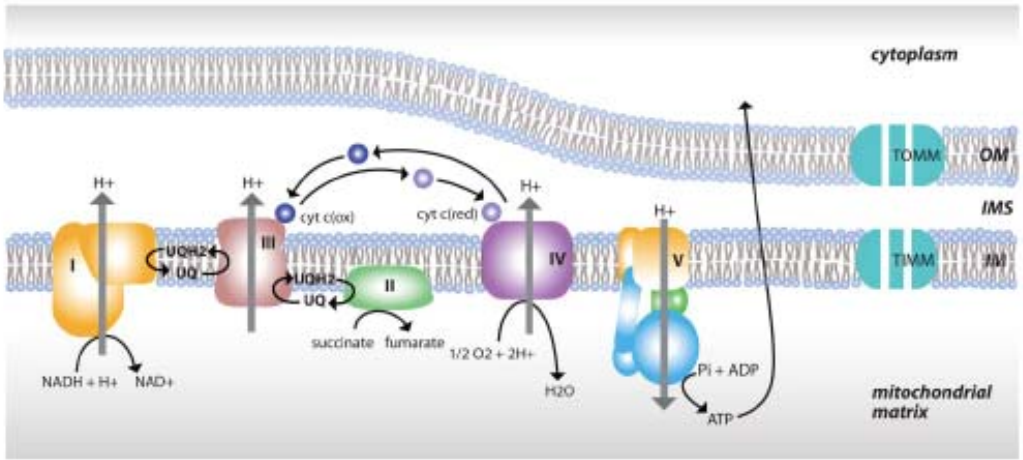

Fig. 1. Altered expression of mitochondrial energy metabolism elements. Energy metabolism-relevant elements showing statistically significant underexpression in the PCC are shown. These elements include the five complexes of the ETC and TIMMs and TOMMs. OM, outer mitochondrial membrane; IMS, intermembrane space; IM, inner mitochondrial membrane.

In particular, the data were used to compare cases and controls in the expression of 80 nuclear genes encoding mitochondrial electron transport chain (ETC) subunits along with translocases of the inner and outer mitochondrial membranes (TIMMs and TOMMs, respectively), in six brain regions. These nuclear genes included 39 complex I genes coding for NADH dehydrogenase, all 4 nuclear-encoded complex II genes coding for succinate dehydrogenase, 9 complex III genes coding for ubiquinol-cytochrome *c* reductase, 13 complex IV genes coding for cytochrome *c* oxidase, and 15 complex V genes coding for ATP synthase, as well as 11 TIMMs and 6 TOMMs, which regulate the transport of nuclear-encoded electron transport subunits into the mitochondria. These ETC complexes and

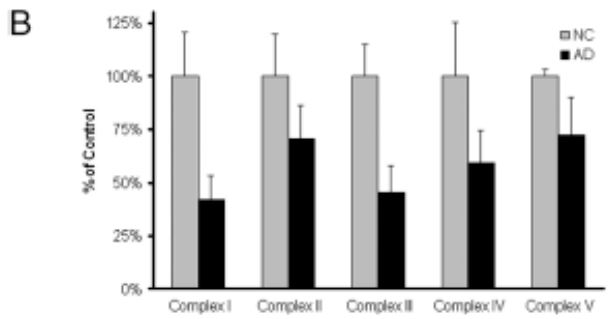

Fig. 2. Western blot validation. (*A*) Western blots using a five-antibody

ASTROCYTE-NEURON LACTATE SHUTTLE

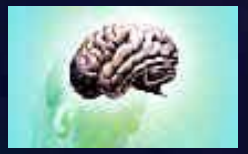

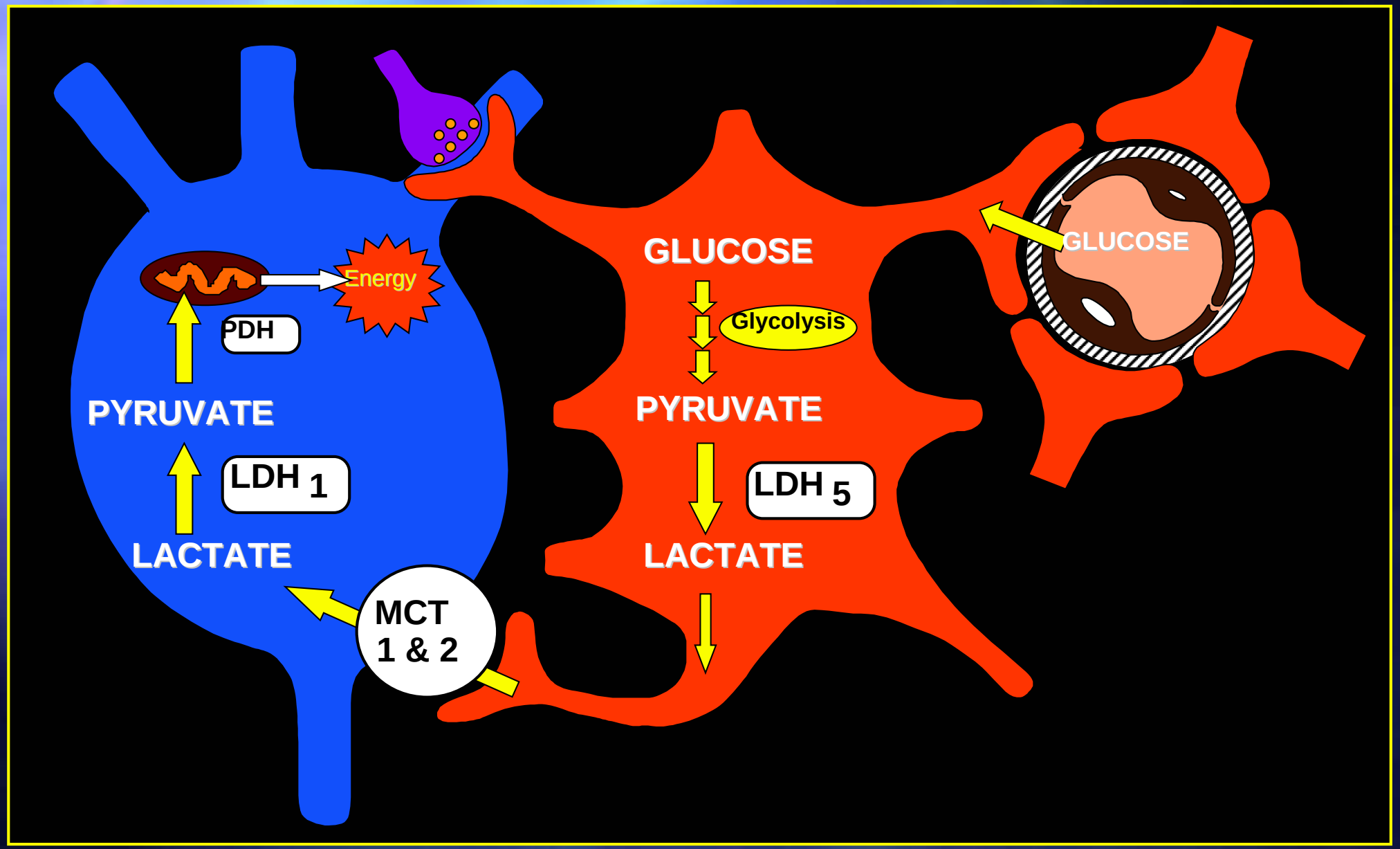

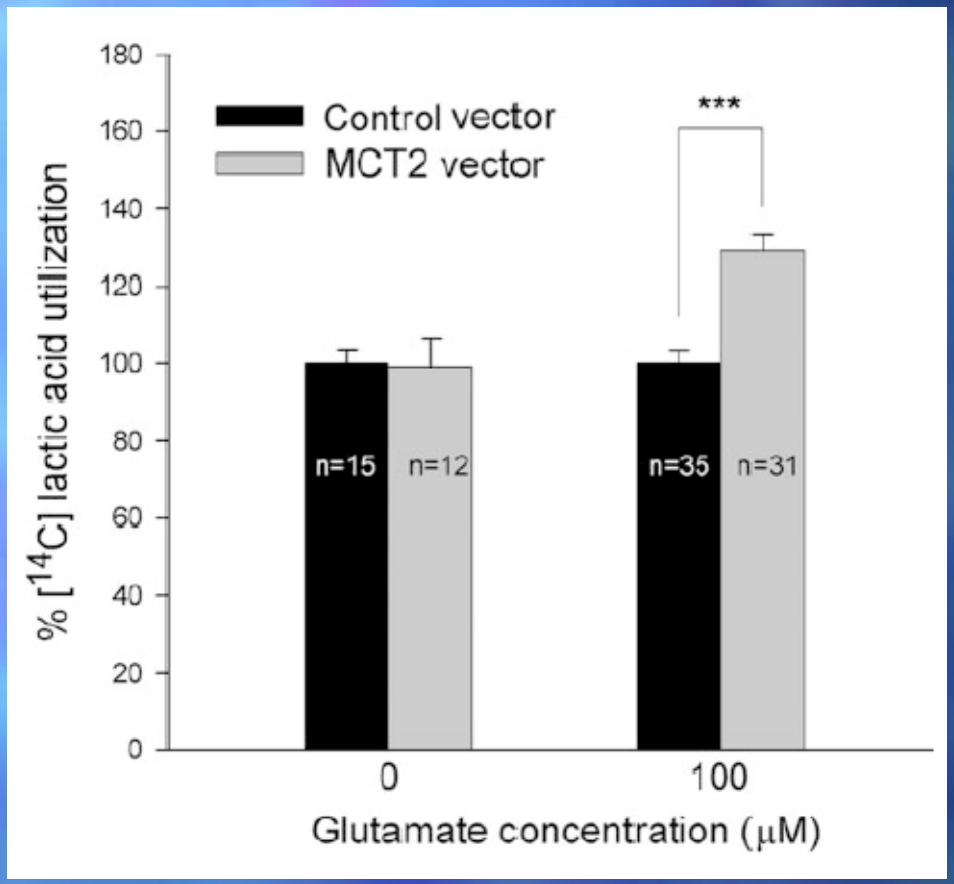

Infection with MCT2 vector increases lactate utilization in the presence of glutamate and 5mM lactate. Data are expressed as a percentage of lactate utilization in the control infected cultures at the same glutamate concentration.

Bliss TM et al. J. of Neuroscience (2004) 24 (27): 6202-6208

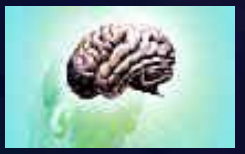

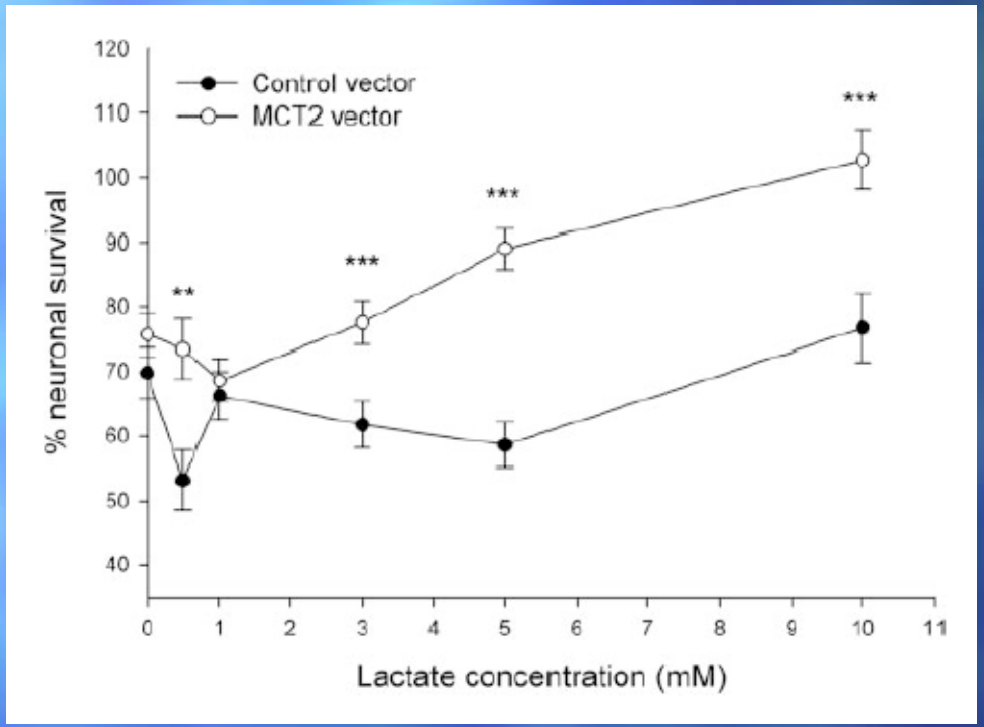

Overexpression of MCT2 protects neurons from an excitotoxic insult.
MCT2-infected hippocampal cultures show greater neuronal survival after a glutamatergic insult (50uM) than control-infected cultures.
Increasing lactate concentration in the cell media significantly increases this neuroprotection in MCT2-infected cultures compared with control-infected cultures.

Bliss TM et al. J. of Neuroscience (2004) 24 (27): 6202-6208

Glia infected with the GLUT1 vector protect neurons from an excitotoxic insult.

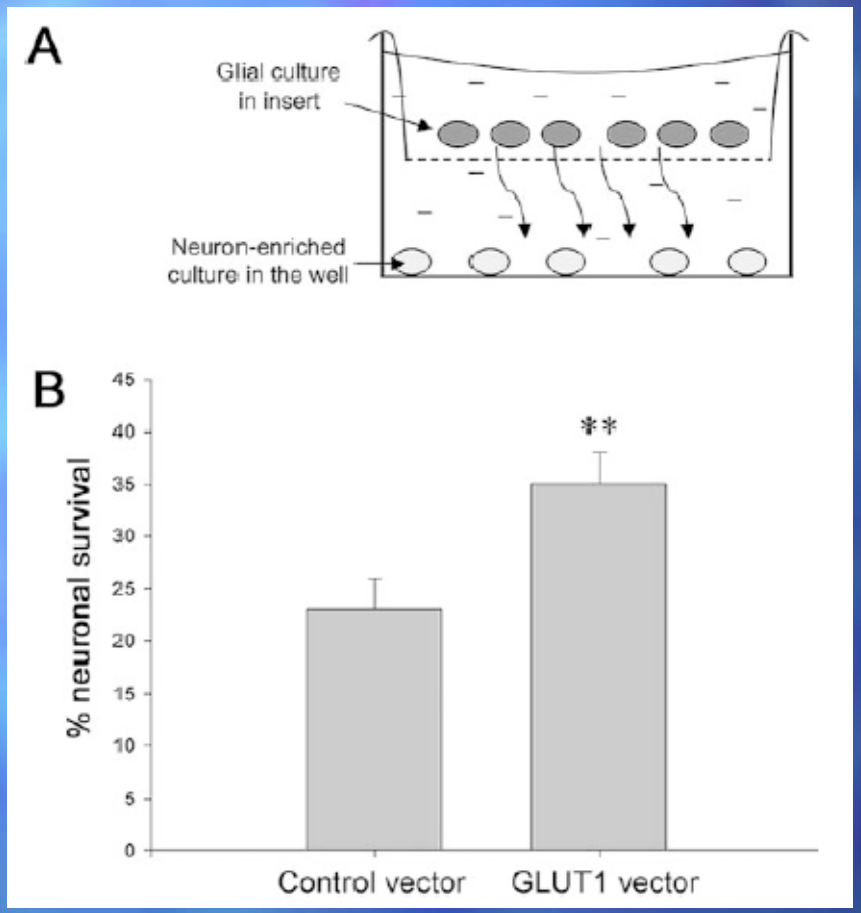

A, Schematic diagram of the laminar culture system. Bent arrows indicate that metabolites released by glia can diffuse to the neurons.
B, Neurons exposed to glia infected with GLUT1 vector show enhanced survival after a gutamatergic insult (LC50 concentration) compared with neurons exposed to glia infected with control vector

Bliss TM et al. J. of Neuroscience (2004) 24 (27): 6202-6208

La transfection combinée de Glut 1 dans les astrocytes et de MCT2 dans les neurones confère une protection vis-à-vis de l'excitotoxicité due au glutamate

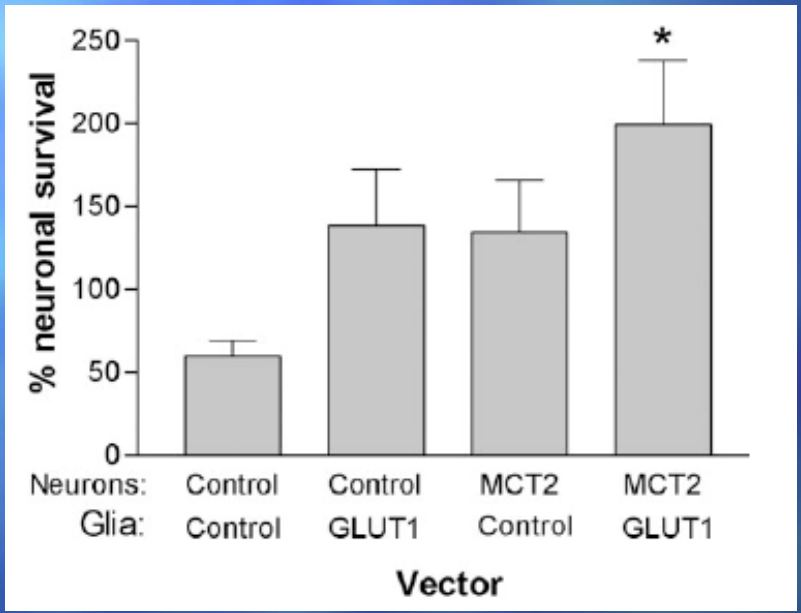

Bliss TM et al. J. of Neuroscience (2004) 24 (27): 6202-6208

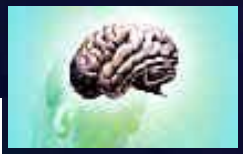

Altered cortical glutamatergic and GABAergic signal transmission with glial involvement in depression

P. V. Choudary*, M. Molnar*, S. J. Evans†, H. Tomita‡, J. Z. Li§, M. P. Vawter‡, R. M. Myers§, W. E. Bunney, Jr.‡, H. Akil†, S. J. Watson†, and E. G. Jones*¶

*Center for Neuroscience and Department of Psychiatry and Behavioral Sciences, University of California, Davis, CA 95616; †Molecular and Behavioral Neuroscience Institute, University of Michigan, Ann Arbor, MI 48109; ‡Department of Psychiatry and Human Behavior, University of California, Irvine, CA 92697; and §Stanford Human Genome Center and the Department of Genetics, Stanford University, Stanford, CA 94305

Contributed by E. G. Jones, September 9, 2005

Table 2. List of candidate genes showing expression changes in MDD and BPD

Gene name	Symbol	Alias	Cytoband	Fold change AnCg	Fold change DLPFC
Major depressive disorder					
Glial high-affinity glutamate transporter, Na^+-dependent	*SLC1A2*	GLT-1; EAAT2	11p13	0.80	0.71
Glial high-affinity glutamate transporter, Na^+-dependent	*SLC1A3*	GLAST; EAAT1	5p13	0.85	0.65
Glutamine synthetase	*GLUL*	GS	1q31	0.73	0.78
Glutamate receptor, ionotropic, AMPA 1	*GRIA1*	AMPA1; IGluR1	5q31.1	1.3	
Glutamate receptor, ionotropic, AMPA 3	*GRIA3*	AMPA3; IGluR3	Xq25		1.18
Glutamate receptor, ionotropic, kainate 1	*GRIK1*	GluR5; EAA3	21q22.11		1.21
Glutamate receptor, ionotropic, kainate 5	*GRIK5*	GluR-KA2; EAA2	19q13.2	1.14	1.21
$GABA_A$ receptor, beta 3	*GABARB3*	$GABA_AR\beta3$	15q11.2		1.21
$GABA_A$ receptor, delta	*GABRD*	$GABA_AR\delta$	1p36.3		1.19
$GABA_A$ receptor, gamma 2	*GABARG2*	$GABA_AR\gamma2$	5q3.1		1.22
Bipolar affective disorder					
Glutamate receptor, ionotropic	*GRIA1*	AMPA1; IGluR1	5q31.1		1.21
Glutamate receptor, ionotropic	*GRIA3*	AMPA3; IGluR3	Xq25	1.21	
Glutamate receptor, ionotropic, kainate 1	*GRIK1*	GluR5; EAA3	21q22.11	0.78	
Glutamate receptor, metabotropic 3	*GRM3*	mGluR3	7q21.1	1.24	1.26
$GABA_A$ receptor, alpha 5	*GABRA5*	$GABA_AR\alpha5$	15q11.2	1.24	1.20
$GABA_B$ receptor 1	*GABBR1*	$GABA_BR1$	6p21.31		1.22

Each record indicates the gene name, symbol, common name, cytoband, and fold changes (FC) of expression in the AnCg and/or DLPFC. Expression values, meeting a significance threshold of $P \leq 0.05$ and a fold change of ≥ 1.175 were considered increases, and those with a fold change of ≤ 0.85 were considered decreases.

Mechanism for Coupling Neuronal Activity to Glucose Utilization

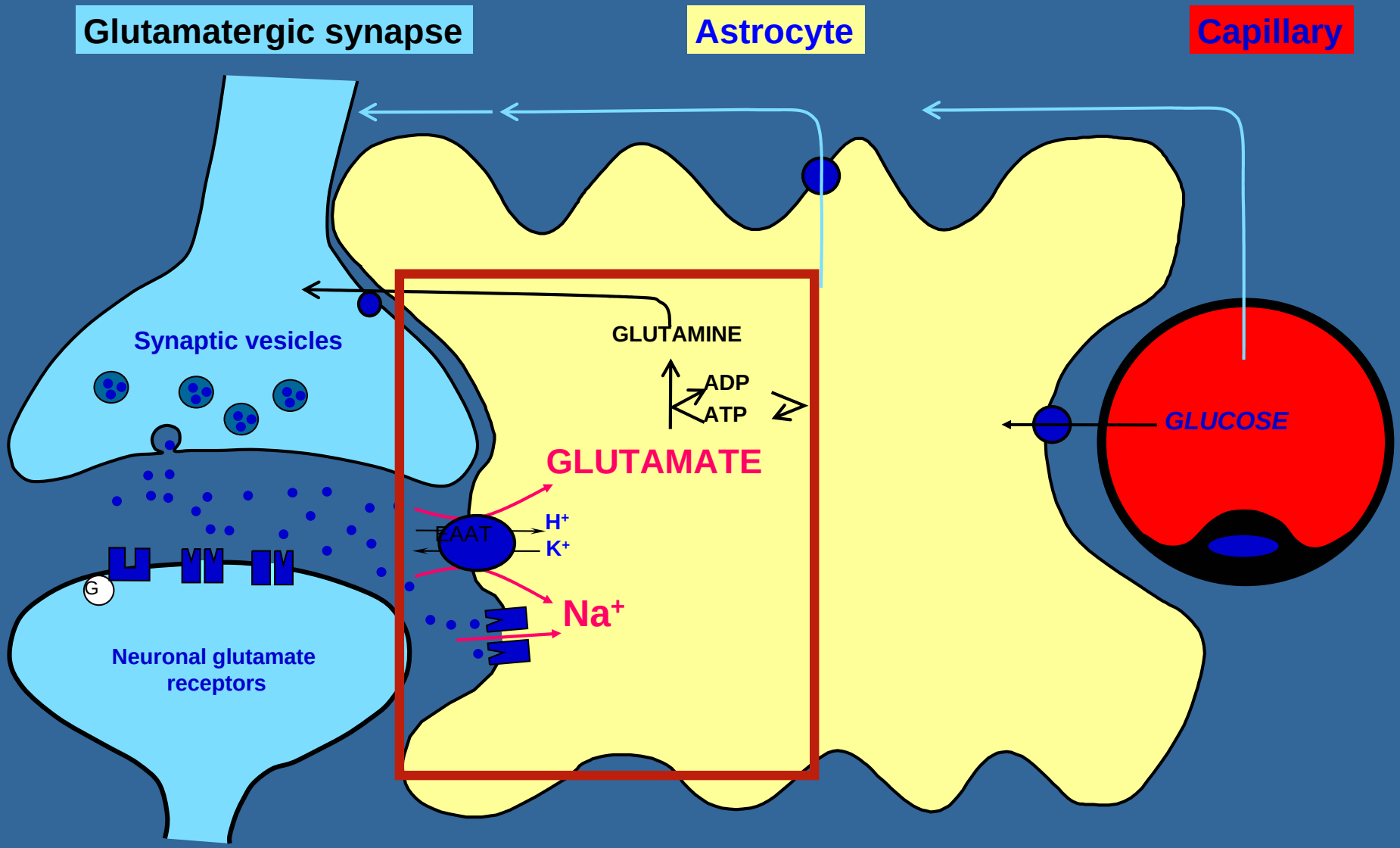

Localisation du cortex préfrontal

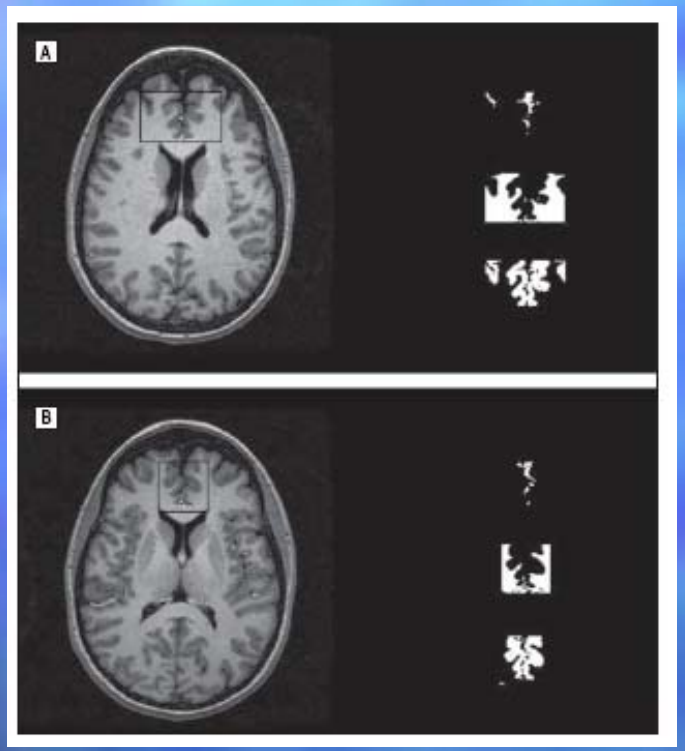

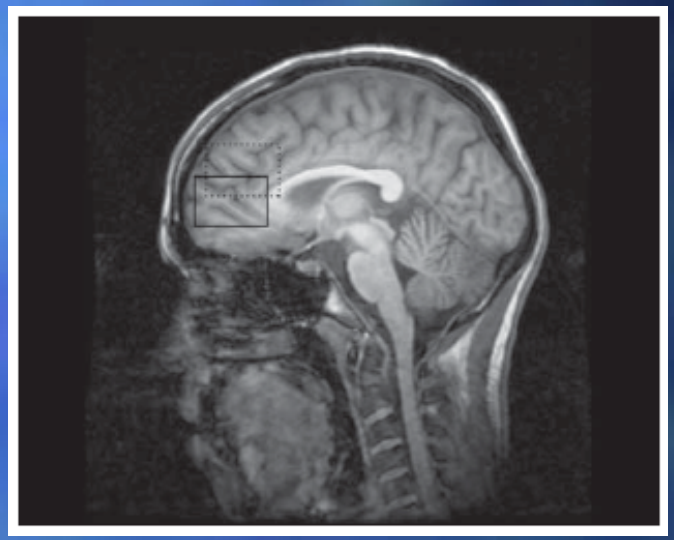

Hasler et al 2007

Deciphering Migraine Mechanisms: Clues from Familial Hemiplegic Migraine Genotypes

Michael A. Moskowitz, MD,[1] Hayrunnisa Bolay, MD, PhD,[2] and Turgay Dalkara, MD, PhD[3]

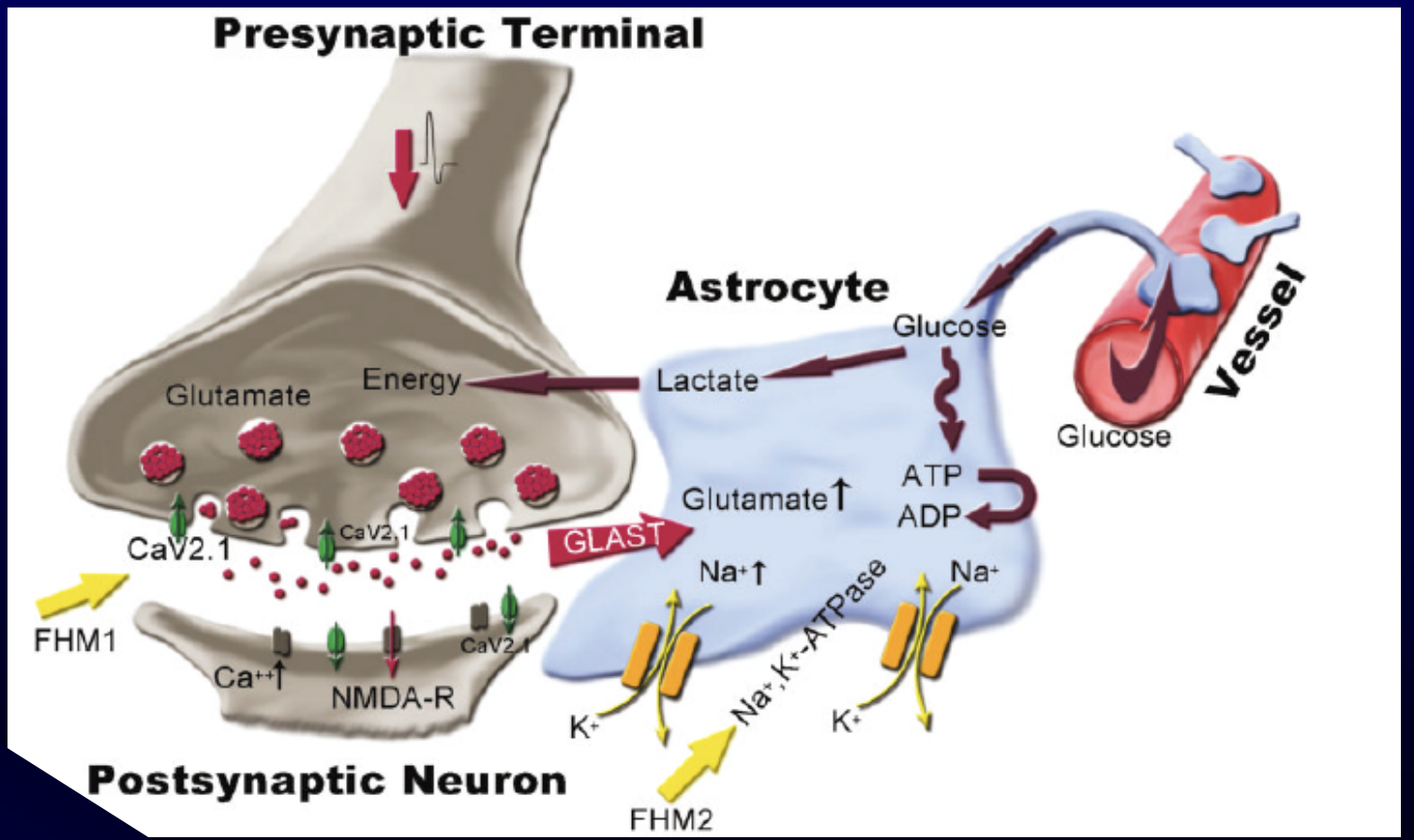

Moskowitz et al 2004

Astrocytes as determinants of disease progression in inherited amyotrophic lateral sclerosis

Koji Yamanaka[1,2], Seung Joo Chun[1], Severine Boillee[1], Noriko Fujimori-Tonou[2], Hirofumi Yamashita[2], David H Gutmann[3], Ryosuke Takahashi[4], Hidemi Misawa[5] & Don W Cleveland[1]

NATURE NEUROSCIENCE VOLUME 11 | NUMBER 3 | MARCH 2008

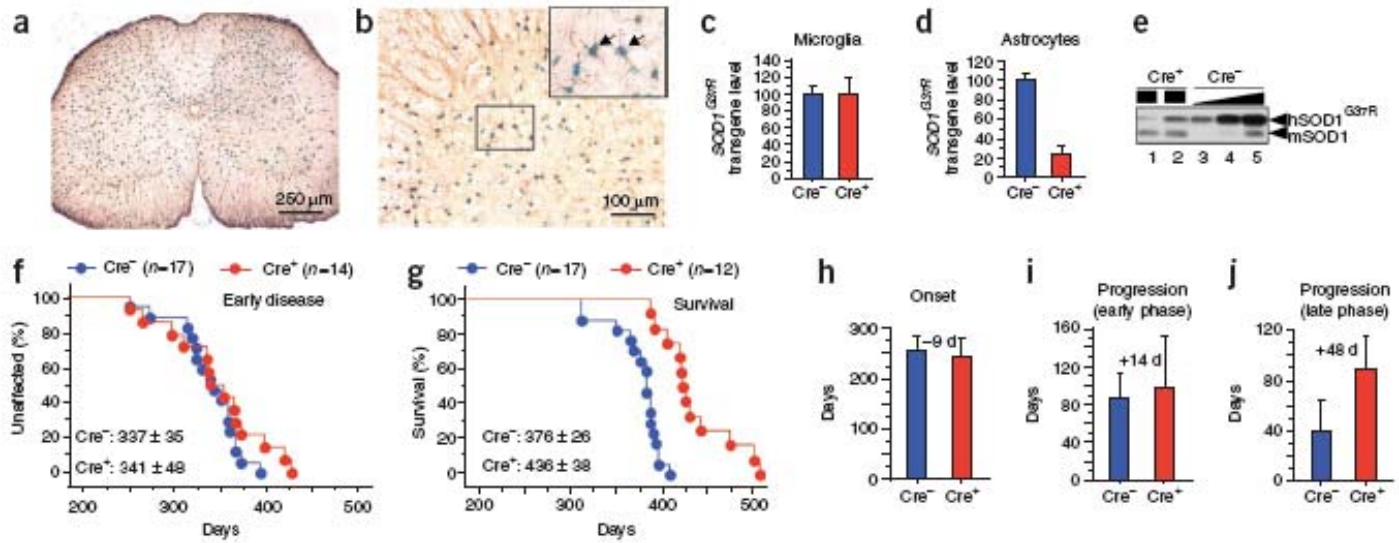

Figure 1 Selective Cre-mediated gene excision shows that mutant SOD1 action in astrocytes is a primary determinant of late disease progression. (a,b) β-galactosidase (β-gal) activity in astrocytes in whole (a) or in the anterior horn region (b) of the lumbar spinal cord section of *GFAP-Cre*/Rosa26 reporter mice visualized with X-gal and immunostaining with GFAP antibody. Inset, magnified image of the boxed area in b. Arrows indicate β-gal/GFAP-Cre–expressing astrocytes. (c,d) *loxSOD1*^{G37R} transgene levels ($n = 3$ for each group) in primary microglia (c) or astrocytes (d) from *loxSOD1*^{G37R}/*GFAP-Cre*$^{+}$ and *loxSOD1*^{G37R} mice using real-time PCR. (e) We determined SOD1^{G37R} and mouse SOD1 levels by immunoblotting extracts from isolated primary astrocytes of *loxSOD1*^{G37R}/*GFAP-Cre*$^{+}$ (lanes 1, 2) and a dilution series of a comparable extract from LoxSOD1^{G37R} astrocytes representing 25%, 50% and 100% of the protein amounts loaded in lanes 1 and 2 (lanes 3–5). (f,g) Ages at which early disease phase (to 10% weight loss, $P = 0.76$; f) or end-stage disease ($P < 0.0001$; g) were reached for *loxSOD1*^{G37R}/*GFAP-Cre*$^{+}$ mice (red) and *loxSOD1*^{G37R} littermates (blue). Mean ages ± s.d. are provided. (h–j) Mean onset ($P = 0.47$) (h), mean duration of early disease (from onset to 10% weight loss, $P = 0.35$; i) and a late disease (from 10% weight loss to end stage, $P < 0.0001$; j) for *loxSOD1*^{G37R}/*GFAP-Cre*$^{+}$ (red) and *loxSOD1*^{G37R} littermates (blue). At each time point, *P* value was determined by unpaired *t*-test. Error bars denote s.d.

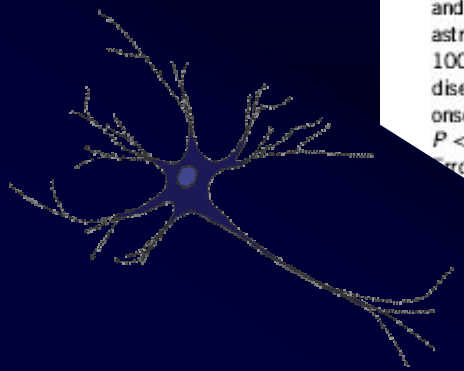

Fig. 6 online). These findings validate therapies, including astrocytic stem cell–replacement approaches, that aim to slow disease progression in ALS by supplementing healthy astrocytes or modulating toxicity in astrocytes to control an inflammatory response of microglia.

Rôle des Astrocytes dans le couplage neurométabolique

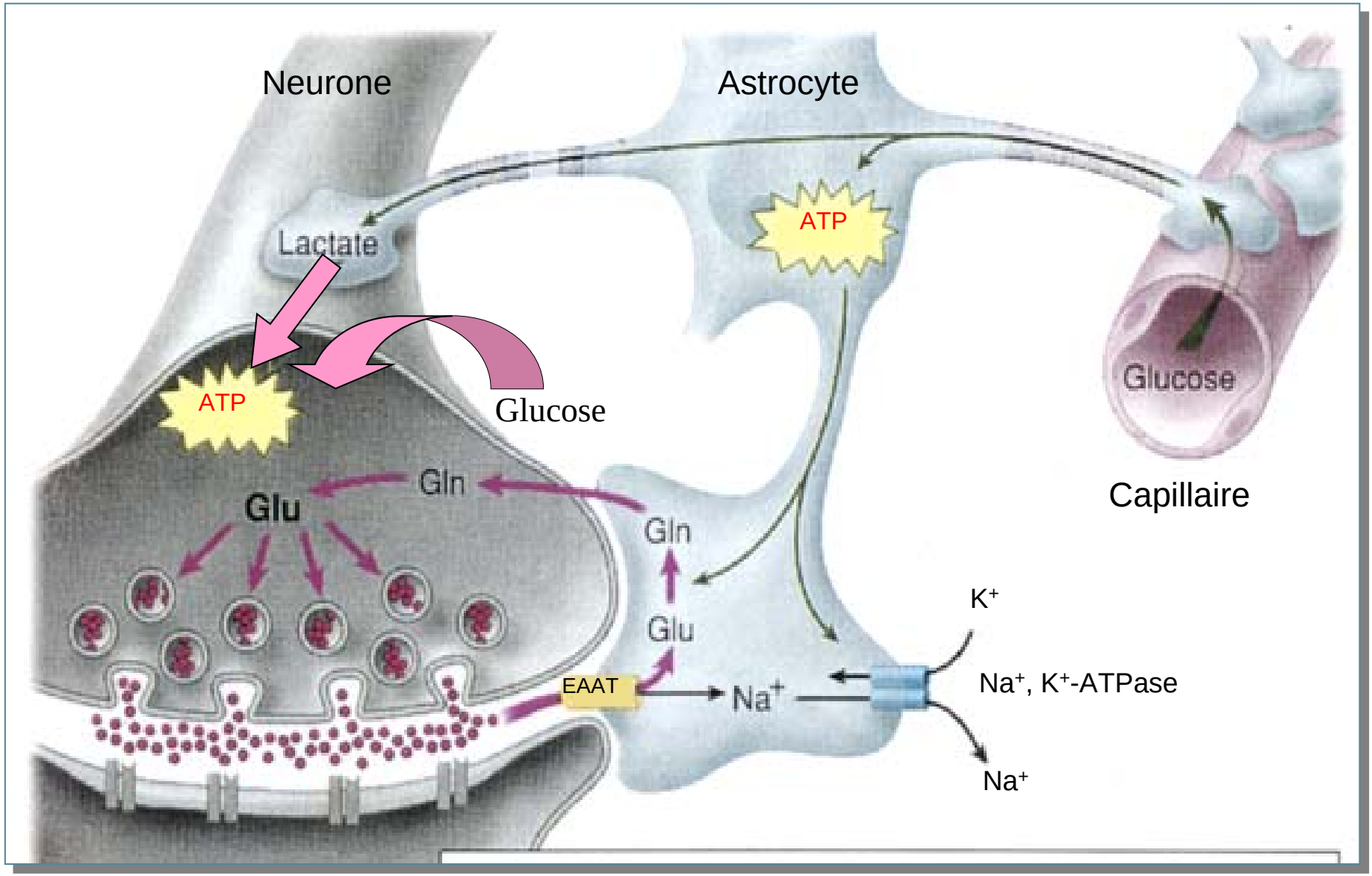

Rôle des astrocytes dans le couplage entre activité synaptique et métabolisme cérébral

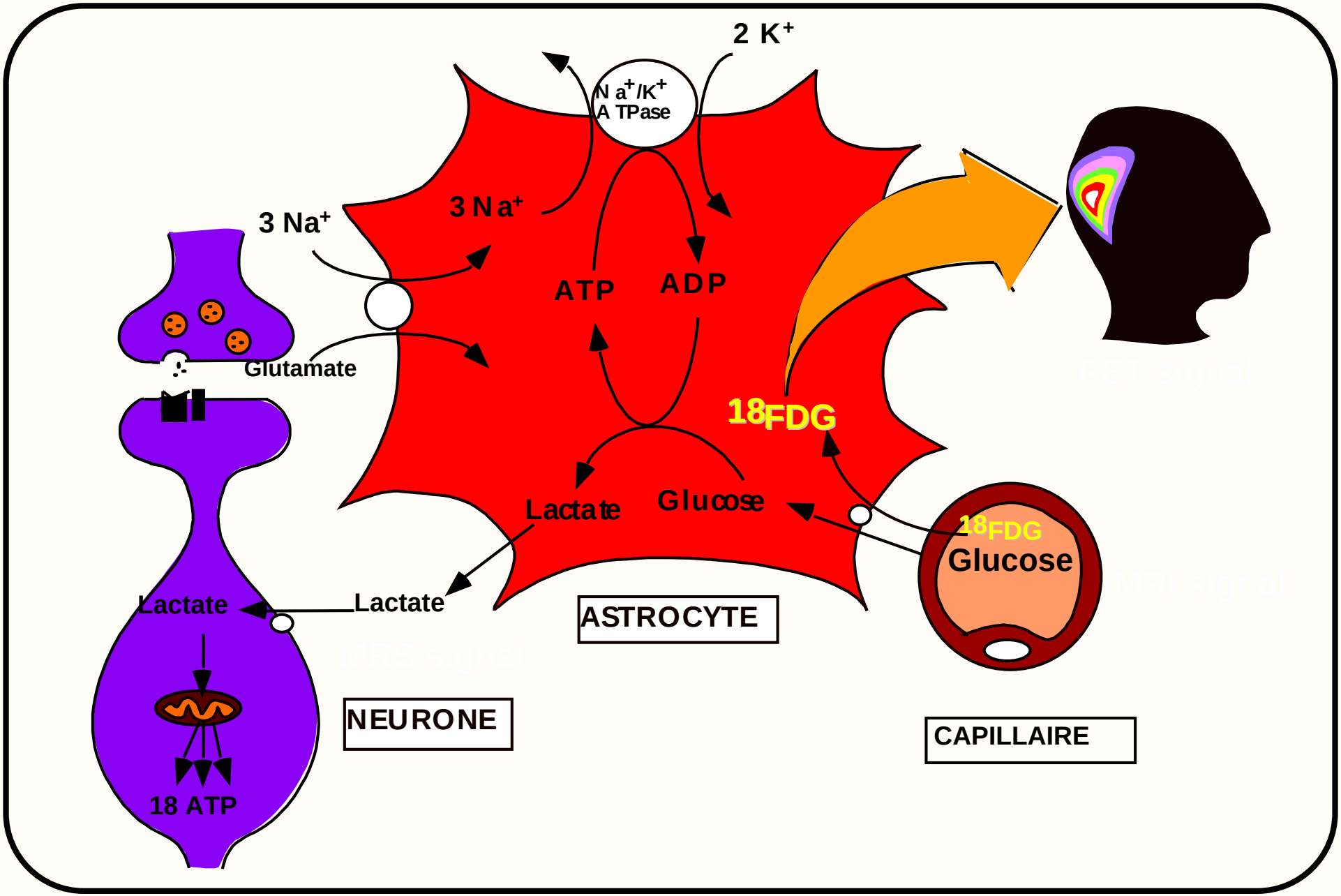

COLLÈGE DE FRANCE
1530

CHAIRE INTERNATIONALE 2007-2008

Pierre Magistretti, professeur

COLLOQUE

Sigmund Freud

NEUROSCIENCES ET PSYCHANALYSE
UNE RENCONTRE AUTOUR DE L'ÉMERGENCE DE LA SINGULARITÉ

Mardi 27 mai 2008
Collège de France
11 place Marcelin-Berthelot - 75005 Paris
amphithéâtre Maurice Halbwachs

Santiago Ramon Y Cajal

Amphithéâtre
Marguerite de Navarre

9h00	Pierre MAGISTRETTI **Accueil et introduction**
9h15	François ANSERMET et Pierre MAGISTRETTI **Plasticité et homéostasie à l'interface entre neurosciences et psychanalyse**
9h50	Cristina ALBERINI **The dymanics of our internal representations : memory consolidation, reconsolidation and the integration of new information with the past**
10h30	pause
10h50	Marcus RAICHLE **Two views of brain function**
11h30	Antonio DAMASIO **A neurobiology for conscious and unconscious processing**
12h10	Jacques-Alain MILLER **Théories des traces** (titre sous réserve)
13h00	pause déjeuner
14h00	Marc JEANNEROD **La psychothérapie neuronale**
14h40	Michel LE MOAL **De l'homéostasie aux processus opposants : une dynamique psychobiologique**
15h20	Alim BENABID **Du Parkinson à l'humeur : le chemin questionnant du neurochirurgien**
16h00	pause
16h20	Daniel WIDLOCHER **Neuropsychologie de l'imaginaire**
17h00	Lionel NACCACHE **De l'inconscient fictif à la fiction consciente**
17h40	Eric LAURENT **Usages des neurosciences pour la psychanalyse**
18h20	Discussion